

$X(3872)$ relevant $D\bar{D}^*$ scattering in $N_f = 2$ lattice QCD

Haozheng Li,^{1,2,*} Chunjiang Shi,^{1,3,†} Ying Chen,^{1,3,‡} Ming Gong,^{1,3} Juzheng Liang,^{1,4} Zhaofeng Liu,^{1,5} and Wei Sun¹

¹*Institute of High Energy Physics, Chinese Academy of Sciences, Beijing 100049, People's Republic of China*

²*School of Physics and Technology, Wuhan University, Wuhan 430072, People's Republic of China*

³*School of Physical Sciences, University of Chinese Academy of Sciences, Beijing 100049, People's Republic of China*

⁴*School of Physics, University of Science and Technology of China, Hefei 230026, People's Republic of China*

⁵*Center for High Energy Physics, Peking University, Beijing 100871, People's Republic of China*

We study the S -wave $D\bar{D}^*(I=0)$ scattering at four different pion masses m_π ranging from 250 MeV to 417 MeV from $N_f = 2$ lattice QCD. Three energy levels $E_{2,3,4}$ are extracted at each m_π . The analysis of $E_{2,3}$ using the effective range expansion (ERE) comes out with a shallow bound state below the $D\bar{D}^*$ threshold, and the phase shifts at $E_{3,4}$ indicate the possible existence of a resonance near 4.0 GeV. We also perform a joint analysis to $E_{2,3,4}$ through the K -matrix parameterization of the scattering amplitude. In this way, we observe a $D\bar{D}^*$ bound state whose properties are almost the same as that from the ERE analysis. At each m_π , this joint analysis also results in a resonance pole with a mass slightly above 4.0 GeV and a width around 40-60 MeV, which are compatible with the properties of the newly observed $\chi_{c1}(4010)$ by LHCb. More scrutinized lattice QCD calculations are desired to check the existence of this resonance.

I. INTRODUCTION

Ever since its discovery in 2003 [1], $X(3872)$ (aka $\chi_{c1}(3872)$ [2]) has been a hot topic in experimental and theoretical studies. It has quantum numbers $I^G J^{PC} = 0^+ 1^{++}$ [3], a mass almost at the $D^0\bar{D}^{0*}$ threshold, and a very tiny width of ~ 1 MeV. It decays mainly into $D^0\bar{D}^{0*}$, and has also decay modes $J/\psi\omega$ ($I=0$) and $J/\psi\rho^0$ ($I=1$) with comparable branching fractions [2]. The exotic properties of $X(3872)$ imply that it is not a pure $\chi_{c1}(2P)$ charmonium whose mass is expected to be above 3.9 GeV [4, 5]. Phenomenological studies also interpret it to be a loosely bound $D\bar{D}^*$ molecule [6–11] (and possibly a small fraction of the $c\bar{c}$ component [12–18]), or a compact tetraquark state [19, 20]. See Refs. [21–26] for reviews.

$X(3872)$ relevant lattice QCD studies observe a strong coupling between $c\bar{c}$ and $D\bar{D}^{(*)}$ [27–29]. This coupling can result in a bound state corresponding to $X(3872)$ below the $D\bar{D}^*$ threshold [28, 29]. However, the study in Ref. [28] does not pay enough attention to the role played by the possible $\chi_{c1}(2P)$ in interpreting the energy levels above the $D\bar{D}^*$ threshold. On the other hand, the $D\bar{D}^*$ interaction can be mediated by light hadrons and therefore can be sensitive to light quark masses. So we will revisit the $X(3872)$ relevant $D\bar{D}^*$ scattering at different pion masses and explore the quark mass dependence of the $D\bar{D}^*$ interaction, which may provide more information to the existing effective field theories describing the $D\bar{D}^*$ interaction [24, 30–33]. In lattice QCD, the $D\bar{D}^*$ scattering amplitude can be derived from the related finite volume energy levels through Lüscher method [34–36]. For the $X(3872)$ relevant $D\bar{D}^*$ scattering, the major numerical challenge is the

calculation of the light quark annihilation diagrams that contribute to the related correlation functions. For this purpose, we adopt the distillation method [37] that provides a sophisticated treatment of both the all-to-all quark propagators and a smearing scheme for quark fields.

II. NUMERICAL DETAILS

We generate $N_f = 2$ gauge configurations at four pion masses ranging from 250 MeV to 417 MeV on $16^3 \times 128$ anisotropic lattices. The aspect ratio is tuned to be $\xi = a_s/a_t \approx 5$, where a_s and a_t are the spatial and temporal lattice spacings, respectively. We adopt the tadpole improved gauge action [38, 39] for gluons and the tadpole improved anisotropic clover fermion action [40–42] for light sea quarks and the valence charm quark. The spatial lattice spacing a_s is set to be $a_s = 0.136(2)$ fm through the Wilson flow method [43, 44]. Then the pion dispersion relation along with the measured ξ are used to determine a_t at each pion mass. The charm quark mass parameter is tuned to give $(m_{\eta_c} + 3m_{J/\psi})/4 = 3069$ MeV. Throughout this study, the correlation functions are calculated using the distillation method [37]. We use $N_V^{(l)} = 70$ in calculating the perambulators for u, d quarks, and $N_V^{(c)} = 120$ in the calculation of charm quark perambulators, where N_V is the number of the eigenvectors of the gauge covariant Laplacian operators on the lattice. The parameters for the gauge ensembles are listed in Table I.

We only consider the possible coupled-channel effects of χ_{c1} states and the S -wave $D\bar{D}^*$ and ignore the coupling from the $J/\psi\omega$ system, which is observed to be very weak (see Ref. [28] and also Appendix A and B). Note that the D -wave ($l = 2$) should also appear in the related $D\bar{D}^*$ scattering. However, its mixing to the S -wave is expected to be suppressed by the phase

* haozhengli2002@gmail.com

† shichunjiang@ihep.ac.cn

‡ chen@ihep.ac.cn

TABLE I. Parameters of the gauge ensembles and the energies of D and D^* with $q = 0, 1$. The non-interacting $D\bar{D}^*$ energies $E_{D\bar{D}^*}^{q=0,1}$ are also shown.

ens.	m_π (MeV)	a_t^{-1}	N_{cfg}	$N_V^{(l)}$	$N_V^{(c)}$	$m_{\chi_{c1}}$ (MeV)	m_D (MeV)	m_{D^*} (MeV)	$E_{D\bar{D}^*}^{q=0}$ (MeV)	$E_D^{q=1}$ (MeV)	$E_{D^*}^{q=1}$ (MeV)	$E_{D\bar{D}^*}^{q=1}$ (MeV)
M245	250(3)	7.276	401	70	120	3489(3)	1873(1)	1985(2)	3858(3)	1958(2)	2064(4)	4022(5)
M305	307(2)	7.187	401	70	120	3496(2)	1881(1)	1990(2)	3871(3)	1962(2)	2070(2)	4032(4)
M360	362(1)	7.187	401	70	120	3502(2)	1884(1)	2003(2)	3888(2)	1970(1)	2084(3)	4054(4)
M415	417(1)	7.219	401	70	120	3509(2)	1896(1)	2017(1)	3913(2)	1978(1)	2094(2)	4072(3)

space factor p^{2l} with p being the scattering momentum and is assumed to be negligible in the practical study [28]. The related interpolating field operators are built in terms of the smeared u, d, c quark fields. The $c\bar{c}$ operators take the spatially extended version, $\mathcal{O}_{c\bar{c}}^r(t) = \frac{1}{N_r} \sum_{|\mathbf{y}-\mathbf{x}|=r} \bar{c}(\mathbf{x}, t) \gamma_5 \gamma_i K_U(\mathbf{x}, \mathbf{y}; t) c(\mathbf{y}, t)$, where

N_r is the multiplicity of $\mathbf{r} = \mathbf{y} - \mathbf{x}$ with $|\mathbf{r}| = r$, and $K_U(\mathbf{x}, \mathbf{y}; t) = \mathcal{P} e^{ig \int_{\mathbf{x}}^{\mathbf{y}} \mathbf{A} \cdot d\mathbf{r}}$ is the Wilson line connecting (\mathbf{y}, t) and (\mathbf{x}, t) (The spatial index i of all the vector operators is omitted for convenience throughout this Letter). Obviously, $\mathcal{O}_{c\bar{c}}^r(t)$ is gauge invariant and has the right quantum number $J^{PC} = 1^{++}$ after the summation over $|\mathbf{r}| = r$. In practice, we use three $\mathcal{O}_{c\bar{c}}^r(t)$ operators (denoted as $\mathcal{O}_{1,2,3}$ in the following) with $r/a_s = 0, 1, 2$, respectively.

The $D\bar{D}^*$ operators with the quantum numbers $I^G J^{PC} = 0^+ 1^{++}$ take the meson-meson operator type

$$\mathcal{O}_{D\bar{D}^*} \sim [(\bar{u}\Gamma_D c)(\bar{c}\Gamma_{D^*} u) - (\bar{u}\Gamma_{D^*} c)(\bar{c}\Gamma_D u)] + (u \rightarrow d), \quad (1)$$

with $(\Gamma_D, \Gamma_{D^*}) = (\gamma_5, \gamma_i)$. S -wave operators are obtained by summing over all the possible directions of the relative momentum, namely, $\mathcal{O}_{AB}^q \sim \sum_{R \in O} \mathcal{O}_A(R \circ \mathbf{q}) \mathcal{O}_B(-R \circ \mathbf{q})$,

where R runs over all the elements of the octahedral group O , and $q = |\mathbf{q}|$ is the magnitude of the relative momentum (in units of $2\pi/L$ with L being the spatial size of the lattice). The operators $\mathcal{O}_{4,6} \equiv \mathcal{O}_{D\bar{D}^*}^{q=0,1}$ are involved in the practical calculation. Another $\mathcal{O}_{D\bar{D}^*}^{q=0}$ operator (labeled as \mathcal{O}_5) uses the combination $(\Gamma_D, \Gamma_{D^*}) = (\gamma_4 \gamma_5, \gamma_4 \gamma_i)$.

A. Finite volume energies

The six operators $\{\mathcal{O}_\alpha, \alpha = 1, 2, \dots, 6\}$ are used to calculate the correlation matrix $C_{\alpha\beta}(t) = \langle 0 | \mathcal{O}_\alpha(t) \mathcal{O}_\beta^\dagger(0) | 0 \rangle$. The practical calculation considers all the quark diagrams, except for those involving the charm quark annihilation. By solving the generalized eigenvalue problem (GEVP), $C_{\alpha\beta}(t) v_\beta^{(n)}(t, t_0) = \lambda^{(n)}(t, t_0) C_{\alpha\beta}(t_0) v_\beta^{(n)}(t, t_0)$ at given t and t_0 , we obtain the optimized correlation function $C^{(n)}(t) = v_\alpha^{(n)} v_\beta^{(n)} C_{\alpha\beta}(t)$ which is contributed mainly by the n -th state. The finite volume energies $E_{2,3,4}$ are extracted through one-exponential fits to the

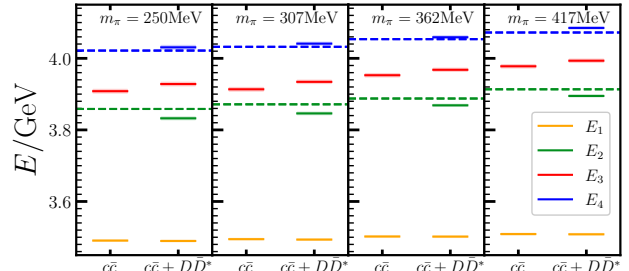


FIG. 1. Energy levels E_n obtained at different m_π . In each panel, the dashed lines show the non-interacting $D\bar{D}^*$ energies $E_{D\bar{D}^*}^{q=0}$ (green) and $E_{D\bar{D}^*}^{q=1}$ (blue) in Table I, while the boxes stand for the finite volume energy levels E_n with their heights indicating statistical errors. In the left column of each panel are the lowest two E_n when only $c\bar{c}$ operators are involved in the GEVP analysis, and the right column includes the lowest four energy levels E_n from all the six operators (\mathcal{O}_{1-6}). It should be noted that there may exist an additional energy level corresponding to the D -wave ($l = 2$) $D\bar{D}^*$ state near the blue dashed line in the figure. Similar to the treatment in Ref. [28], we tentatively neglect the mixing from the D -wave wave state to the S -wave, which is expected to be suppressed by the phase space factor p^{2l} particularly for the low-energy $D\bar{D}^*$ scattering [48]. The effect of this kind of mixing needs to be explored by involving more $D\bar{D}^*$ operators.

ratio functions [45–47]

$$R_n(t) = \frac{C^{(n)}(t)}{C_D(t, q) C_{D^*}(t, q)} \approx A e^{-\Delta_n t}, \quad (2)$$

where $C_{D^{(*)}}(t, q)$ is the correlation function of $D^{(*)}$ with a momentum $q = 0, 1$, and $\Delta_n = E_n - E_{D\bar{D}^*}^q$ is the difference of E_n from the nearest non-interacting $D\bar{D}^*$ energy. In practice, we use $q = 0$ for $E_{2,3}$ and $q = 1$ for E_4 . We also perform two-exponential fits to $C^{(n)}(t)$ in proper time windows for a self-consistent check in Appendix C. All the statistical errors are obtained through the jackknife method.

The obtained finite volume energy levels are illustrated in Fig. 1 by colored boxes, whose heights indicate the statistical errors. In each panel labeled by m_π , the yellow and red boxes in the left column are the two energy levels that are derived from the GEVP analysis involving only the $c\bar{c}$ operators ($\mathcal{O}_{1,2,3}$). The lowest level is roughly 3.5 GeV and corresponds to the conventional charmonium χ_{c1} , while the second level is higher than 3.9 GeV and coincides with the quark model expectation of the $\chi_{c1}(2P)$ mass [4, 5, 49–52]. Note that this energy may

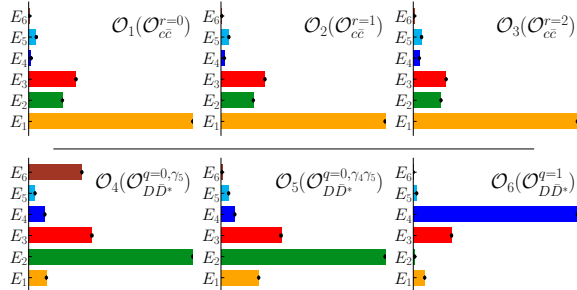


FIG. 2. Relative couplings $Z_\alpha^{(n)} = \langle 0 | \mathcal{O}_\alpha | n \rangle$ at $m_\pi = 417$ MeV. For each operator \mathcal{O}_α , $Z_\alpha^{(n)}$ is normalized by the largest value in $\{Z_\alpha^{(n)}, n = 1, 2, \dots, 6\}$. For each state $|n\rangle$, $Z_\alpha^{(n)}$ (in the same color) signal the relative importance of $c\bar{c}$ and $D\bar{D}^*$ components.

not be an eigenvalue of the lattice Hamiltonian. When the $\mathcal{O}_{D\bar{D}^*}$ operators $\mathcal{O}_{4,5,6}$ are added, more energy levels are obtained. The colored boxes in the right-hand side of each column in Fig. 1 show the lowest four energy levels (labeled E_1, E_2, E_3, E_4 from bottom up). E_1 is almost the same as the lowest level obtained by $c\bar{c}$ operators. The second lowest level E_2 (green box) appears close to but right below the non-interacting $D\bar{D}^*$ energy $E_{D\bar{D}^*}^{q=0}$ (green dashed line), and E_4 lies right above the non-interacting $D\bar{D}^*$ energy $E_{D\bar{D}^*}^{q=1}$ (blue dashed line) (see Table I for the exact values). It is interesting to see that E_3 resides in the middle of $E_{D\bar{D}^*}^{q=0}$ and $E_{D\bar{D}^*}^{q=1}$.

$E_{1,2,3,4}$ are taken to be the eigenvalues of the lattice Hamiltonian relevant to 0^+1^{++} charmonium-like systems. The relative couplings of \mathcal{O}_α to different states $Z_\alpha^{(n)} = |\langle 0 | \mathcal{O}_\alpha | n \rangle|$ (normalized by the largest value in each panel) are illustrated in Fig. 2. Obviously, the $c\bar{c}$ operators $\mathcal{O}_{1,2,3}$ couple most to the E_1 state and also have substantial overlaps to the E_2 and E_3 states. In contrast, $\mathcal{O}_{4,5}$ ($D\bar{D}^*$ operators with $q = 0$) couple mainly to E_2 , and also overlap substantially to E_1 and E_3 states. \mathcal{O}_6 ($\mathcal{O}_{D\bar{D}^*}(q = 1)$ operator) couples predominantly to E_4 and has a sizable coupling to the E_3 state. The E_1 state is naturally the $\chi_{c1}(1P)$ state. The E_2 and E_3 states are from the mixing of $\chi_{c1}(2P)$ and non-interacting $D\bar{D}^*$ state of $q = 0$, which pulls E_2 downwards below the $D\bar{D}^*$ threshold (apart from the possible attractive interaction of $D\bar{D}^*$ due to meson exchanges) and pushes E_3 upwards, as exactly shown in Fig. 1. It is expected that E_4 is slightly above the non-interacting energy $E_{D\bar{D}^*}^{q=1}$ due to the mixing from $\chi_{c1}(2P)$. It should be noted that the D -wave $D\bar{D}^*$ scattering state can have a $J^{PC} = 1^{++}$ quantum number and is degenerate with the S -wave state in the non-interacting limit. The S - D -wave mixing (and also the possible different mixing from $\chi_{c1}(2P)$) may result in two energy levels near $E_{D\bar{D}^*}^{q=1}$ (the blue dashed line in Fig. 1). By assuming the contribution from the D -wave state is negligible, as indicated in the lattice QCD calculation of the $T_{cc}^+(3875)$ relevant DD^* scattering [48, 53], we use only one operator $\mathcal{O}_{D\bar{D}^*}(q = 1)$ that resembles the S -wave $D\bar{D}^*$ scattering state and

makes the second energy level indiscernible. The effect of this kind of mixing needs to be explored by involving more $D\bar{D}^*$ operators at $q = 1$.

Strictly speaking, E_2, E_3, E_4 are the energy levels of the $D\bar{D}^*$ scattering states in a finite box and are related to the corresponding scattering amplitude through Lüscher's formula [34–36] for the S -wave scattering

$$p \cot \delta_0(p) = \frac{2}{\sqrt{\pi}L} \mathcal{Z}_{00}(1; q^2), \quad q^2 \equiv \left(\frac{L}{2\pi}\right)^2 p^2, \quad (3)$$

where p is the scattering momentum defined through $E_n(p_n) = \sqrt{m_D^2 + p_n^2} + \sqrt{m_{D^*}^2 + p_n^2}$ for each E_n . Table II collects the results of $(p^2, p \cot \delta_0(p))$ of $E_{2,3,4}$ at all the four values of m_π , where the statistical errors are obtained by jackknife analyses. However, there are subtleties in the derivation of $p \cot \delta_0$ for E_2 . The $D\bar{D}^*$ scattering may include the interaction from one pion exchange (OPE), which introduces nonanalyticity to $p \cot \delta_0(p)$ when p^2 is below the left-hand cut (lhc) point $(p_{\text{lhc}}^{1\pi})^2 = ((m_{D^*} - m_D)^2 - m_\pi^2)/4$ [54–56].

B. Bound state and the possible lhc issue

The values of $(p_{\text{lhc}}^{1\pi})^2$ at different m_π 's are also shown in Table II. It is seen that $p^2(E_2) > (p_{\text{lhc}}^{1\pi})^2$ is satisfied only for $m_\pi = 417(1)$ MeV. So we discuss the near-threshold $D\bar{D}^*$ scattering amplitude at $m_\pi = 417(1)$ MeV following the strategy in Ref. [28, 57], since the $p \cot \delta_0(p)$ derived at E_2 and E_3 from Eq. (3) are valid. The effective range expansion (ERE), $p \cot \delta_0(p) = \frac{1}{a_0} + \frac{1}{2}r_0 p^2$, at E_2 and E_3 gives two equations with two unknowns, namely, the S -wave scattering length a_0 and the effect range r_0 . The solutions are

$$a_0 = -4.0(1.0) \text{ fm}, \quad r_0 = 0.187(38) \text{ fm}, \quad (4)$$

where the large negative a_0 signals the existence of a bound state. Taking these values as the approximation of those in the infinite volume, the scattering amplitude $t \propto (p \cot \delta_0(p) - ip)^{-1}$ implies a bound state pole at $p_B = i\kappa_B$ with $\kappa_B = 49.8_{-18.2}^{+17.0}$ MeV. Consequently, we get the binding energy E_B ,

$$E_B = E_{D\bar{D}^*}(p_B) - (m_D + m_{D^*}) = -1.3_{-1.0}^{+0.8} \text{ MeV}. \quad (5)$$

Weinberg's compositeness criterion states that a near-threshold bound state can be viewed as an admixture of a compact state and a two-hadron channel. According to the generalized Weinberg relation in Ref. [58], the small positive r_0 indicates the compositeness $X \approx 1$ up to $O(p^2)$. Therefore, this bound state is predominantly a $D\bar{D}^*$ bound state.

If the same procedure is applied to cases at other m_π 's, then similar results can be obtained, as shown in Table II. The “binding energy” $E_B = -9.7_{-2.2}^{+2.1}$ MeV at $m_\pi = 250(3)$ MeV is also consistent with the value $11(7)$ MeV obtained in Ref. [28] at $m_\pi \approx 266$ MeV.

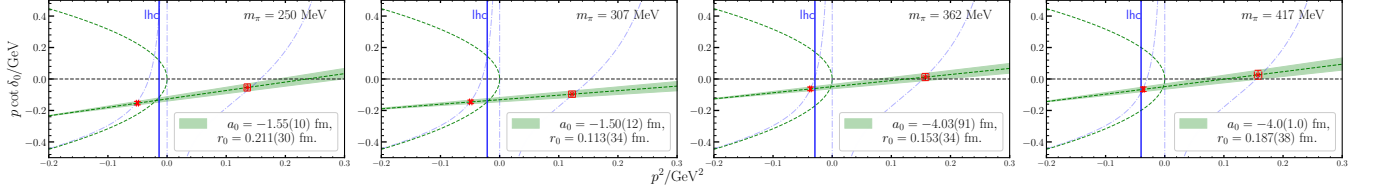


FIG. 3. Phase shifts of S-wave $J^{PC} = 1^{++} DD^*$ system and effective range expansion fitting. The red data points illustrate phase shifts $p \cot \delta_0(q)$ obtained from $(E_{2,3})$, while the green bands show the related effective ranges expansion. The background dashed lines present the Riemann-Zeta function trajectory.

TABLE II. DD^* scattering parameters. The scattering momentum p^2 , the phase shift $p \cot \delta_0(p)$ (and δ_0) at $E_{2,3,4}$, as well as the lhc point $(p_{\text{lhc}}^{1\pi})^2 \approx \frac{1}{4}[(m_D - m_{D^*})^2 - m_\pi^2]$, are given explicitly at four values of m_π . The energy shifts Δ_n (derived from Eq. (2)) of E_n from the nearby non-interacting energy of DD^* are also presented. Also collected are the derived scattering length a_0 , the effective range r_0 from E_2, E_3 , and the estimated binding energy E_B (and binding momentum $p_B = +i|p_B|$) for the bound state pole. The from the K -matrix parameters and the resulted bound state information are also shown for comparison. The asterisks in brackets ‘(*)’ indicate that the corresponding values may be problematic when OPE lhc is considered.

	m_π (MeV)	250(3)	307(2)	362(1)	417(1)
E_4	Δ_4 (MeV) = $E_4 - E_{DD^*}^{q=1}$	9.1(1.3)	8.9(1.2)	5.3(1.3)	12.8(1.3)
	p^2 (GeV ²)	0.339(8)	0.335(6)	0.340(6)	0.342(4)
	$p \cot \delta_0(p)$ (GeV)	-2.02(66)	-2.35(65)	-2.76(89)	-1.79(28)
	δ_0	(163.9 ^{+4.0} _{-7.3})°	(166.1 ^{+3.0} _{-5.1})°	(168.1 ^{+2.9} _{-5.5})°	(161.9 ^{+7.4} _{-3.2})°
E_3	Δ_3 (MeV) = $E_3 - E_{DD^*}^{q=0}$	70(3)	63(3)	80(3)	80(3)
	p^2 (GeV ²)	0.135(5)	0.122(6)	0.158(6)	0.158(6)
	$p \cot \delta_0(p)$ (GeV)	-0.054(19)	-0.097(19)	0.012(22)	0.026(24)
	δ_0	(98.4 ^{+3.3} _{-3.6})°	(105.4 ^{+3.0} _{-3.1})°	(88.2 ^{+3.3} _{-3.3})°	(86.2 ^{+4.0} _{-4.1})°
E_2	Δ_2 (MeV) = $E_2 - E_{DD^*}^{q=0}$	-26.1(9)	-25.4(11)	-19.0(7)	-18.6(8)
	p^2 (GeV ²)	-0.050(2)	-0.049(2)	-0.037(1)	-0.036(1)
	$p \cot \delta_0(p)$ (GeV)	-0.154(9)(*)	-0.146(10)(*)	-0.063(11)(*)	-0.066(13)
	$(p_{\text{lhc}}^{1\pi})^2$ (GeV ²)	-0.0135(4)	-0.0210(4)	-0.0292(3)	-0.0400(3)
$(E_{2,3})$	a_0 (fm)	-1.55(10)(*)	-1.50(12)(*)	-4.03(91)(*)	-4.0(1.0)
	r_0 (fm)	0.211(30)(*)	0.113(34)(*)	0.153(34)(*)	0.187(38)
	p_B (MeV)	+i 137(9)(*)	+i 137(11)(*)	+i 50(11)(*)	+i 50(13)
	E_B (MeV)	-9.7 ^{+2.1} _{-2.2} (*)	-9.7 ^{+1.9} _{-2.0} (*)	-1.3 ^{+0.6} _{-0.8} (*)	-1.3 ^{+0.8} _{-1.0}
K -matrix $(E_{2,3,4})$	M (MeV)	3948(6)(*)	3981(11)(*)	3960(11)(*)	3979(10)
	γ	-381(22)(*)	-468(43)(*)	-750(101)(*)	- 677(90)
	g (GeV ²)	-220(14)(*)	-205(25)(*)	-565(97)(*)	- 532(94)
	p_B (MeV)	+i 146(9)(*)	+i 141(10)(*)	+i 57(11)(*)	+i 58(12)
	E_B (MeV)	-11(1)(*)	-10(2)(*)	-1.7(7)(*)	-1.7(7)

However, the p^2 of E_2 for these m_π 's are lower than the corresponding $(p_{\text{lhc}}^{1\pi})^2$ and make the derived $p \cot \delta_0(p)$ at E_2 questionable. Refs. [54, 55] discuss the OPE lhc effect on the $T_{cc}^+(3875)$ relevant DD^* scattering using the lattice data in Ref. [48] and find that, except for the singular behavior that $p \cot \delta_0(p)$ bends up abruptly when p^2 approaching $(p_{\text{lhc}}^{1\pi})^2$ from above, the overall p^2 behavior is similar to that of ERE including the values of p^2 below $(p_{\text{lhc}}^{1\pi})^2$. Figure 3 shows the phase shifts (red points), as well as ERE of $p \cot \delta_0(p)$ (green bands) for the four m_π 's. In each panel, the ERE curve intersects with the bound state curve ip (dashed green line). If the DD^* scattering also has the similar feature to that of the $DD^*(I=0)$ scattering when considering the OPE lhc, then it is possible that $p \cot \delta_0(p)$ has also a pole near the lhc point $(p_{\text{lhc}}^{1\pi})^2$ (red dashed vertical line) and exhibits a rapid increase there to intersect earlier with the bound state curve ip at $p^2 > (p_{\text{lhc}}^{1\pi})^2$. Therefore, it is very likely that there exists a bound state pole at each m_π with a

smaller $|E_B|$ than the value in Table II.

C. Possible resonance

Possible resonance.— Now we consider the physical implication of the energy level E_3 , which lies in the middle of the DD^* threshold and $E_{DD^*}^{q=1}$. In Ref. [28], the E_3 state is interpreted as the upward shifted DD^* state with the relative momentum $q=0$ owing to the formation of a bound state below the threshold. The physical consideration behind this is Levinson's theorem that, when n_l bound states are formed in the l partial wave, the phase shift satisfies the relation $\delta_l(p=0^+) = n_l\pi$ with the convention $\delta(p=\infty) = 0$. However, when there exist n_b confined channels (with discretized energies) between the threshold and a specific momentum p_{max} , one should use the generalized Levinson's theorem $\delta_l(0^+) - \delta_l(p_{\text{max}}) = (n_l - n_b)\pi$ [59, 60]. For the case at

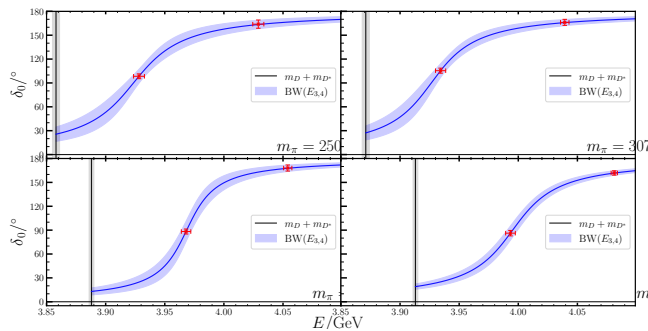


FIG. 4. The S -wave $D\bar{D}^*$ scattering phase δ_0 at $E_{3,4}$ and the Breit-Wigner parameterization. In each panel of the figure, the red data points represent the phase shifts at E_3 and E_4 at each m_π (see Table II). The vertical line indicates the $D\bar{D}^*$ threshold. The blue bands (labelled by $BW(E_{2,3})$) illustrate the resonance using parameters (m_R, Γ_R) from $E_{2,3}$ based on the Breit-Wigner ansatz in Eq. (6).

hand with $n_0 = 1$ and the possible existence of $\chi_{c1}(2P)$ (the confined channel) expected by quark models, $\delta_0(p)$ will undergo an evolution that it starts from π at $p = 0^+$ ($\cot \delta_0(0^+) = \lim_{p \rightarrow 0^+} 1/(a_0 p) \rightarrow -\infty$ for $a_0 < 0$), falls down when the energy increases, and then return to π when the energy passes the $\chi_{c1}(2P)$ mass, as is exactly the case (see the values of the phase shift $\delta_0 \rightarrow 180^\circ$ at E_4 in Table II). It is stressed that $E_4 > E_{D\bar{D}^*}^{q=1}$ is crucial for this reasoning. Actually, this phase change also hints at the existence of a resonance. The Breit-Wigner ansatz for a resonance (m_R, Γ_R) gives

$$\delta_0(E) = \arctan\left(\frac{\Gamma_R}{2(m_R - E)}\right). \quad (6)$$

Using $\delta_0(E_3)$ and $\delta_0(E_4)$ as inputs, the resonance parameters (m_R, Γ_R) at each m_π are estimated and are collected in Table III. Figure 4 illustrates the evolution of $\delta_0(E)$ with respect to the center-of-mass energy E of $D\bar{D}^*$, where red points are the lattice data, the blue bands are plots of Eq. (6) with parameters in Table III, and the dashed lines indicate the possible phase change below the resonant energy E_R . Since they are tentatively estimated from only two lattice energy levels, the resonance parameters (m_R, Γ_R) may change if more scrutinized lattice investigations are performed.

Phenomenological studies also indicate that when the coupled-channel effect of $D\bar{D}^*$ and the quark model $\chi_{c1}(2P)$ is considered, apart from a narrow structure near the $D^0\bar{D}^{*0}$ threshold, there may exist a wide resonance below 4.0 GeV with the width ranging from 17 to 80 MeV [13, 61–65]. These observations are compatible with the results of this study. Experimentally, $X(3940)$ reported by Belle in 2007 [66, 67] has the resonance parameters $(m_X, \Gamma) \sim (3942(9), 37_{-17}^{+27})$ MeV, and decays mainly into $D\bar{D}^*$ but not $D\bar{D}$, and therefore favors the assignment of a 1^{++} resonance. However, it is puzzling that a similar structure has not been observed by other experiments yet.

TABLE III. Bound state and resonance parameters. The first group of the data lists the resonance parameters (m_R, Γ_R) from $E_{3,4}$ are obtained by Eq. (6). The second group shows the pole parameters and the pole residuals of the bound state pole through the K -matrix parameterization of the phase shifts at $E_{2,3,4}$. The third group gives the resonance parameters as well as the resonance coupling $|c_0|^2$ to $D\bar{D}^*$, the partial decay width $\Gamma_{D\bar{D}^*}$ and the corresponding branching ratio.

m_π (MeV)	250(3)	307(2)	362(1)	417(1)
BW fit from $E_{3,4}$				
m_R (MeV)	3924(5)	3926(6)	3969(4)	3995(4)
Γ_R (MeV)	63(23)	57(18)	37(13)	57(10)
Bound state pole and residue from $E_{2,3,4}$				
Imp_B (MeV)	+i 146(9)	+i 141(10)	+i 57(11)	+i 58(12)
E_B (MeV)	-11(1)	-10(2)	-1.6(7)	-1.7(7)
c_0^2 (GeV ²)	62(4)	58(4)	23(5)	24(5)
c_0 (GeV)	7.9(3)	7.6(3)	4.8(5)	4.9(5)
\hat{g}	2.04(7)	1.97(8)	1.23(12)	1.24(14)
Resonance pole and residue from $E_{2,3,4}$				
Rep_R (MeV)	545(4)	559(6)	569(4)	563(4)
Imp_R (MeV)	-i 56(6)	-i 34(8)	-i 38(7)	-i 45(7)
m_R (MeV)	4008(4)	4029(4)	4050(3)	4071(3)
Γ_R (MeV)	60(6)	38(9)	43(8)	50(7)
$ c_0 ^2$ (GeV ²)	47(5)	28(7)	32(6)	38(6)
$ c_0 $ (GeV)	6.9(4)	5.3(6)	5.6(5)	6.1(5)
\hat{g}	1.71(9)	1.32(17)	1.39(13)	1.51(12)
$\Gamma_{D\bar{D}^*}$ (MeV)	63(6)	39(9)	44(8)	51(8)
$Br_{D\bar{D}^*}$ (%)	~ 100	~ 100	~ 100	~ 100

D. Joint analysis on $E_{2,3,4}$

We also perform a joint analysis based on the energy levels $E_{2,3,4}$. The K -matrix parameterization is applied to describe the single channel S -wave $D\bar{D}^*$ scattering amplitude t at $E_{2,3,4}$, namely,

$$t_0(s) = \frac{K(s)}{1 - K(s)i\rho(s)}, \quad (7)$$

where s is the invariant mass squared of $D\bar{D}^*$, $\rho(s)$ is the two-body phase space factor $\rho(s) = p/(8\pi\sqrt{s})$, and $K(s)$ is a real function of s , such that the unitary condition

$$\text{Im}t_0^{-1}(s) = -\rho(s) = -\frac{1}{16\pi} \frac{2p}{\sqrt{s}} \Theta(\sqrt{s} - E_{\text{thr.}}), \quad (8)$$

is satisfied for $s > E_{\text{thr.}}$ with $E_{\text{thr.}} = m_D + m_{D^*}$. In the case of this study, we have the relation

$$p \cot \delta_0(p(s)) = 16\pi \frac{\sqrt{s}}{2} K^{-1}(s). \quad (9)$$

As shown in Fig. 5, the phase shift we obtain indicates $p \cot \delta_0(p) \approx 0$ near $p^2(E_3)$, so we parameterize $K(s)$ as

$$K(s) = \frac{g}{M^2 - s} + \gamma \quad (10)$$

with M, g, γ being free real parameters, where the single pole term is introduced to account for the possible zero

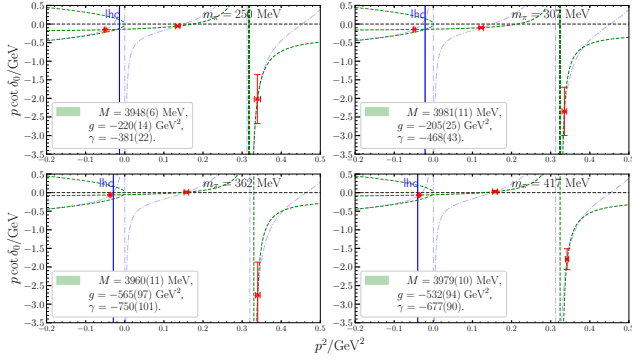


FIG. 5. Phase shifts at E_2, E_3, E_4 and the K -matrix parameterization. The layout is similar to that of Fig. 3. The green bands illustrate the K -matrix expression of $p \cot \delta_0(p)$ K -matrix in Eq. 9.

of $K^{-1}(s)$. Thus we tentatively solve the equation given by Eqs. (9) and (10) to determine these parameters using the values of $p \cot \delta_0(p)$ at $E_{2,3,4}$. The obtained parameters M, g, γ at the four values of m_π are listed in Table II, where the errors are obtained through the jackknife analysis.

The green bands in Fig. 5 illustrate the function form in Eq. (9) with the determined parameters. It is seen that the green bands intersect with the lower branch of the parabola (green dashed line) and indicate the possible existence of a bound state for each m_π . By solving the pole equation $p \cot \delta_0(p) = ip$ in the physical sheet, we obtain positive imaginary values of p_B and therefore negative binding energies $E_B < 0$ for the bound states at the four m_π , which are also listed in Table II. The values of E_B are compatible with the results from the $E_{2,3}$ through ERE. The tiny slopes of the green bands near the threshold also indicate small positive effective ranges r_0 (if ERE is applicable in this region), which also imply the compositeness $X \approx 1$ of the bound states. Let $s_0 = (m_D + m_{D^*} + E_B)^2$ be the bound state pole position in s -plane, then close to the pole, the scattering amplitude t has the asymptotic behavior

$$t_0(s \approx s_0) = \frac{c_0^2}{s_0 - s}, \quad (11)$$

with the pole residual c_0^2 giving the coupling of the bound state to DD^* . With the parameterization of $K(s)$ in Eq. (10) and performing a contour integral around s_0 , we obtain positive values of c_0^2 , which give the couplings

$$\begin{aligned} c_0(m_\pi \approx 250 \text{ MeV}) &= 7.9(3) \text{ GeV} \\ c_0(m_\pi \approx 307 \text{ MeV}) &= 7.6(3) \text{ GeV} \\ c_0(m_\pi \approx 362 \text{ MeV}) &= 4.8(5) \text{ GeV} \\ c_0(m_\pi \approx 417 \text{ MeV}) &= 4.9(5) \text{ GeV}. \end{aligned} \quad (12)$$

By assuming a pure bound state for $X(3872)$ (the compositeness $X \approx 1$), an effective field theory study

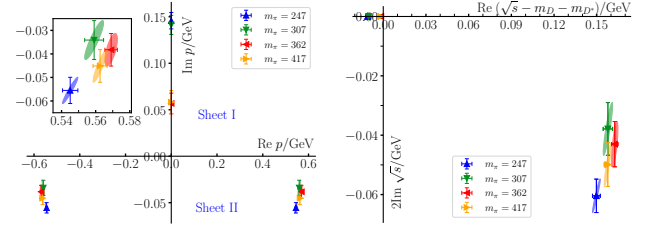


FIG. 6. Pole positions in the complex p -plane (left) and \sqrt{s} -plane (right). Only physical poles are shown. The bound state poles reside on the positive imaginary axis of the p -plane (left) and the negative real axis of \sqrt{s} -plane (right). The points in the lower half of the p -plane (left) and the sight-bottom \sqrt{s} -plane illustrate the resonance poles.

comes out with the effective coupling [68]

$$c_0^2 \approx \frac{16\pi}{\mu} \sqrt{\frac{2|E_B|}{\mu}} (m_D m_{D^*} \sqrt{s_0}), \quad (13)$$

with $\mu = (m_D + m_{D^*})/(m_D m_{D^*})$ being the reduced mass of the DD^* system, which gives $c_0 \approx (10.6^{+0.3}_{-0.3}, 10.4^{+0.5}_{-0.6}, 6.7^{+0.6}_{-0.8}, 6.7^{+0.6}_{-0.8})$ GeV at the four pion masses $m_\pi = (250, 307, 362, 417)$ MeV. These values are qualitatively compatible with those in Eq. (12) from the pole residuals. In addition, these bound state poles also pass the sanity check that the S -matrix satisfies the asymptotic behavior $S(p \approx p_B) \approx \frac{-ig_B^2}{p - p_B}$ with $g_B^2 = c_0^2 \mu / \sqrt{s_0} > 0$ [69].

With the parameters M, g, γ , we check if there exist resonance poles by solving the pole equation $p(s) \cot \delta_0(p(s)) - ip(s) = 0$ in the unphysical Riemann sheet with $\text{Im} p(s) < 0$. A pair of conjugate resonance poles $\sqrt{s_0} = m_R \pm i \frac{\Gamma_R}{2}$ are obtained for each m_π ,

$$\begin{aligned} (m_R, \Gamma_R)(m_\pi \approx 250 \text{ MeV}) &= (4008(4), 60(6)) \text{ MeV} \\ (m_R, \Gamma_R)(m_\pi \approx 307 \text{ MeV}) &= (4029(4), 38(9)) \text{ MeV} \\ (m_R, \Gamma_R)(m_\pi \approx 362 \text{ MeV}) &= (4050(3), 43(8)) \text{ MeV} \\ (m_R, \Gamma_R)(m_\pi \approx 417 \text{ MeV}) &= (4071(3), 50(7)) \text{ MeV}, \end{aligned} \quad (14)$$

whose positions in the complex p -plane and \sqrt{s} -plane are illustrated in Fig. 6. We also use Eq. (11) to extract the resonance coupling c_0 at the pole $s \approx s_0$ and obtain complex values of c_0^2 at different m_π . Their modulus $|c_0|^2, |c_0|$ and the corresponding dimensionless coupling $\hat{g} = |c_0|/m_R$ are collected in Table III. With the coupling $|c_0|^2$ of the resonance R to DD^* , the partial decay width $\Gamma_{D\bar{D}^*}$ is predicted using

$$\Gamma_{D\bar{D}^*} = |c_0|^2 \frac{\rho(m_R^2)}{m_R}, \quad (15)$$

which are also listed in Table III. It is seen that, for all the four m_π , we have $\Gamma_{D\bar{D}^*} \approx \Gamma_R$, which implies that the decay branching fraction $\Gamma_{D\bar{D}^*}/\Gamma_R$ is almost 100%, as is expected since DD^* is the only open-charm decay channel permitted by the kinematics and symmetries.

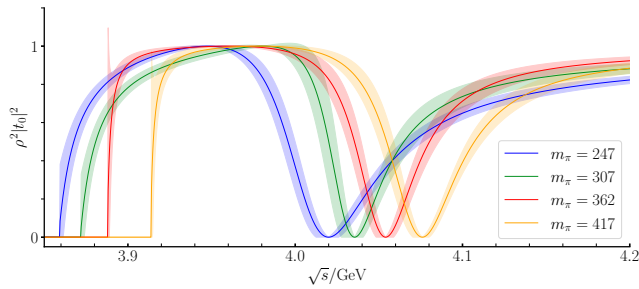


FIG. 7. Amplitudes $\rho^2|t_0|^2$ for the four pion masses. The zero values of $\rho^2|t_0|^2$ signal the presence of the CDD zero [70] due to the existence of additional components (the quark model $\chi_{c1}(2P)$ for example).

We also plot in Fig. 7 the squared $D\bar{D}^* \rightarrow D\bar{D}^*$ scattering amplitude $\rho^2|t_0|^2$ for $\sqrt{s} > E_{\text{thr.}}$. For each m_π , the zero value of $\rho^2|t_0|^2$ is due to the well-known Castillejo-Dalitz-Dyson (CDD) zero [70] of the amplitude t_0 , which signals the possible existence of an additional component other than the $D\bar{D}^*$ system (the quark model $\chi_{c1}(2P)$ for instance) [71]. We notice that a model study on the two-particle scattering shows the presence of the CDD zero when there exists a bare state in the relevant energy region [60]. Theoretically, the vanishing t_0 at the CDD zero can be attributed to the cancellation of the $D\bar{D}^*$ self-interaction and the $D\bar{D}^*-\chi_{c1}(2P)$ interaction owing to the interplay of hadron and quark degrees of freedom [17, 72–76]. The positions m_{CDD} of the CDD zeros for the four values of m_π are determined to be

$$\begin{aligned} m_{\text{CDD}}(m_\pi \approx 250 \text{ MeV}) &= 4020(3) \text{ MeV} \\ m_{\text{CDD}}(m_\pi \approx 306 \text{ MeV}) &= 4036(3) \text{ MeV} \\ m_{\text{CDD}}(m_\pi \approx 362 \text{ MeV}) &= 4054(3) \text{ MeV} \\ m_{\text{CDD}}(m_\pi \approx 417 \text{ MeV}) &= 4076(2) \text{ MeV}, \end{aligned} \quad (16)$$

which are very close to the corresponding resonance masses m_R and imply a close connection of the resonance with the possible quark model $\chi_{c1}(2P)$.

The LHCb collaboration recently reported the clear observation of a 1^{++} charmoniumlike state $\chi_{c1}(4010)$ with the resonance parameters $(m_{\chi_{c1}}, \Gamma_{\chi_{c1}} = (4012.5^{+3.6+4.1}_{-3.9-3.7}, 62.7^{+7.0+6.4}_{-6.4-6.6}) \text{ MeV}$ [77]. It is amazing that the resonance parameters we obtain in Eq. (14) are in quite good agreement with $\chi_{c1}(4010)$. We are not sure at present whether this coincidence of the lattice QCD result and the experiment is accidental or a glimpse of the truth. After all, we have only three finite volume energy levels $E_{2,3,4}$ at hand, it is not the time to draw a sound conclusion until more scrutinized lattice QCD studies on this topic are performed in the future.

III. SUMMARY

We calculate the $I^G J^{PC} = 0^{+1^{++}}$ channel $D\bar{D}^*$ scattering at four pion masses ranging from 250 MeV

to 417 MeV in $N_f = 2$ lattice QCD. We use the distillation method to calculate the related correlation matrix of $c\bar{c}$ operators and $D\bar{D}^*$ operators and obtain three energy $E_{2,3,4}$ levels around the $D\bar{D}^*$ threshold. At $m_\pi \approx 417 \text{ MeV}$ where there are no severe OPE lhc issues, a normal ERE analysis to the two energy levels $E_{2,3}$ results in a shallow bound state, which resides below the $D\bar{D}^*$ by $1.3^{+0.8}_{-1.0} \text{ MeV}$ and has a compositeness $X \approx 1$ indicating a predominant $D\bar{D}^*$ component. The phase shifts $p \cot \delta_0(p)$ at $E_{3,4}$ indicate the possible existence of a resonance below 4.0 GeV.

We also perform a joint analysis of the three energy levels $E_{2,3,4}$ through the K -matrix parameterization of the scattering amplitude. After solving the pole equation in the physical Riemann sheet, a genuine bound state is obtained, whose properties are similar to those of the bound state derived through the ERE analysis. This bound state can correspond to $X(3872)$. In addition, we observe a resonance pole in the second Riemann sheet with a mass slightly higher than 4.0 GeV and a width of 40-60 MeV. This resonance decays into $D\bar{D}^*$ by almost 100%. It is interesting to note that the properties of this resonance are in fairly good agreement with the newly observed $\chi_{c1}(4010)$ by LHCb [77]. Anyway, we remark that this result should be checked by more sophisticated lattice QCD calculations in the future with more finite volume energy levels from more lattice volumes and more kinetic frames [78–80].

ACKNOWLEDGMENTS

We are grateful to Profs. Qiang Zhao, Feng-Kun Guo, Jia-Jun Wu, Zhihui Guo and Xu Feng for the valuable discussions. This work is supported by the National Natural Science Foundation of China (NNSFC) under Grants No. 11935017, No. 12293060, No. 12293061, No. 12293065, No. 12293063, No. 12075253, No. 12070131001 (CRC 110 by DFG and NNSFC), No. 12175063, No. 12205311, the National Key Research and Development Program of China (No. 2020YFA0406400) and the Strategic Priority Research Program of Chinese Academy of Sciences (No. XDB34030302). The Chroma software system [81] and QUDA library [82, 83] are acknowledged. The computations were performed on the HPC clusters at the Institute of High Energy Physics (Beijing), China Spallation Neutron Source (Dongguan), and the ORISE computing environment.

Appendix A: Conventions and Operators

These appendix provide further information on our study on the $D\bar{D}^*(I = 0)$ scattering process. The contents include the details of the operators' construction, the calculation of correlation matrix, and the derivation of finite volume energy levels, etc.

We take the following procedure to build $D\bar{D}^*$ operators with quantum numbers $I^G J^{PC} = 0^+ 1^{++}$. According to the isospin assignment of u, d quarks,

$$\begin{cases} |u\rangle = |\frac{1}{2}, \frac{1}{2}\rangle, \\ |d\rangle = |\frac{1}{2}, -\frac{1}{2}\rangle, \end{cases} \quad \begin{cases} |\bar{d}\rangle = |\frac{1}{2}, \frac{1}{2}\rangle, \\ |\bar{u}\rangle = -|\frac{1}{2}, -\frac{1}{2}\rangle, \end{cases} \quad (\text{A1})$$

we have the isospin states of D and D^* ,

$$\begin{cases} |D^{(*)+}\rangle = |c\bar{d}\rangle = |\frac{1}{2}, \frac{1}{2}\rangle, \\ |D^{(*)0}\rangle = |c\bar{u}\rangle = -|\frac{1}{2}, -\frac{1}{2}\rangle, \\ |\bar{D}^{(*)0}\rangle = |u\bar{c}\rangle = |\frac{1}{2}, \frac{1}{2}\rangle, \\ |D^{(*)-}\rangle = |d\bar{c}\rangle = |\frac{1}{2}, -\frac{1}{2}\rangle. \end{cases} \quad (\text{A2})$$

Thus the $I = 0$ combination of charge neutral $D\bar{D}^*$ states reads

$$|D\bar{D}^*\rangle_{I=0}^{Q=0} = \frac{1}{2} (|D^+ \bar{D}^{*0}\rangle + |D^0 \bar{D}^{*+}\rangle - |\bar{D}^0 D^{*0}\rangle - |D^- D^{*+}\rangle). \quad (\text{A3})$$

Since the charge conjugation transformation (\mathcal{C}) of D and D^* are conventionally defined as $\mathcal{C}|D\rangle = +|\bar{D}\rangle$, $\mathcal{C}|D^*\rangle = -|\bar{D}^*\rangle$, one can easily check the \mathcal{C} transformation $\mathcal{C}|D\bar{D}^*\rangle_{I=0}^{Q=0} = +|D\bar{D}^*\rangle_{I=0}^{Q=0}$. The \mathcal{P} -parity $P = +$ requires the $D\bar{D}^*$ relative angular momentum $l = 0$. Therefore, the S -wave $D\bar{D}^*$ state with the combination in Eq. (A3) has the desired quantum numbers $I^G J^{PC} = 0^+ 1^{++}$. The combination in Eq. (A3) gives also the flavor structure of the interpolation field operator of $D\bar{D}^*$ systems.

A S -wave two-particle operator $\mathcal{O}_{AB}(q)$ is easily constructed by summing over all the relative momenta $\mathbf{p} \equiv 2\pi\mathbf{q}/L$ with the same $q = |\mathbf{q}|$, namely,

$$\mathcal{O}_{AB}^q = \frac{1}{N_q} \sum_{R \in O} \mathcal{O}_A(R \circ \mathbf{q}) \mathcal{O}_B(-R \circ \mathbf{q}). \quad (\text{A4})$$

where R runs over all the elements of the octahedral group O and N_q is the degeneracy of q .

Based on the operator set introduced above,

$$\mathcal{S} = \{\mathcal{O}_\alpha | \alpha = 1, \dots, 7\} = \{\mathcal{O}_{c\bar{c}}^{r=0}, \mathcal{O}_{c\bar{c}}^{r=1}, \mathcal{O}_{c\bar{c}}^{r=2}, \mathcal{O}_{D\bar{D}}^{\mathbf{q}=0, \gamma_5}, \mathcal{O}_{D\bar{D}}^{\mathbf{q}=0, \gamma_4 \gamma_5}, \mathcal{O}_{D\bar{D}}^{\mathbf{q}=1}, \mathcal{O}_{J/\psi\omega}^{q=0}\}, \quad (\text{B1})$$

we calculate the corresponding correlation matrix

$$C_{\alpha\beta}(t) = \frac{1}{T} \sum_{\tau} \langle \mathcal{O}_\alpha(t + \tau) \mathcal{O}_\beta(\tau) \rangle \quad (\alpha, \beta = 1, 2, \dots, 7), \quad (\text{B2})$$

where the correlation functions with different source time slices τ are averaged to increase the statistics. Figure A1 shows the quark diagrams after Wick's contraction that are involved in the calculation of $C_{\alpha\beta}(t)$. All the con-

Given the single-particle operators of D and \bar{D}^* , $(\mathcal{O}_D, \mathcal{O}_{D^*}) \equiv (\bar{u}(d)\Gamma_{DC}, \bar{u}(d)\Gamma_{D^*c})$, we combine the relations in Eq. (A3) and (A4) to build up the $D\bar{D}^*$ operators $\mathcal{O}_{D\bar{D}^*}^q$ with the quantum numbers $I^G J^{PC} = 0^+ 1^{++}$. In practice, we use two combinations of Γ_D and Γ_{D^*} , namely, $(\Gamma_D, \Gamma_{D^*}) = (\gamma_5, \gamma_i)$ and $(\gamma_4 \gamma_5, \gamma_4 \gamma_i)$. The operators $\mathcal{O}_{D\bar{D}^*}^{q=0, \gamma_5(\gamma_4 \gamma_5)}$ with the two (Γ_D, Γ_{D^*}) combinations (indicated by the superscripts γ_5 and $\gamma_4 \gamma_5$) are also named by \mathcal{O}_4 and \mathcal{O}_5 , respectively. The $\mathcal{O}_{D\bar{D}^*}^{q=1}$ operator uses the first (Γ_D, Γ_{D^*}) combination and is also named as \mathcal{O}_6 .

The S -wave $J/\psi\omega$ operator with $q = 0$ is simply the antisymmetric combination of the single particle operators $\mathcal{O}_{J/\psi}^j(q = 0)$ and $\mathcal{O}_\omega^k(q = 0)$, namely, $\mathcal{O}_7 \equiv \mathcal{O}_{J/\psi\omega}^{q=0} \rightarrow \epsilon_{ijk} \mathcal{O}_{J/\psi}^j(q = 0) \mathcal{O}_\omega^k(q = 0)$.

For the convenience of discussions, we recite the build-up of $c\bar{c}$ operators presented in the main text. Since the χ_{c1} mass $m_{\chi_{c1}} \approx 3.51$ GeV is far from the energy region relevant to $X(3872)$, we need several $c\bar{c}$ operators to distinguish states of interest from χ_{c1} . So we build several spatially extended charmonium $c\bar{c}$ operators

$$\mathcal{O}_{c\bar{c}}^r(t) = \frac{1}{N_r} \sum_{|\mathbf{y}-\mathbf{x}|=r} \bar{c}(\mathbf{x}, t) \gamma_5 \gamma_i K_U(\mathbf{x}, \mathbf{y}; t) c(\mathbf{y}, t), \quad (\text{A5})$$

where N_r is the multiplicity of $\mathbf{r} = \mathbf{y} - \mathbf{x}$ with $|\mathbf{r}| = r$, and

$$K_U(\mathbf{x}, \mathbf{y}; t) = \mathcal{P} e^{ig \int_{\mathbf{y}}^{\mathbf{x}} \mathbf{A} \cdot d\mathbf{r}} \quad (\text{A6})$$

is a Wilson line connecting (\mathbf{y}, t) and (\mathbf{x}, t) . Obviously, $\mathcal{O}_{c\bar{c}}^r(t)$ is gauge invariant and has the right quantum number $J^{PC} = 1^{++}$ (actually T_1^{++} on the lattice) after the summation over $|\mathbf{r}| = r$. In practice, we use three $\mathcal{O}_{c\bar{c}}^r(t)$ operators (denoted by $\mathcal{O}_{1,2,3}$) with $r/a_s = 0, 1, 2$, respectively.

Appendix B: Determination of finite volume energies

nected quark diagrams and the diagrams including the light quark annihilation effects are taken into account, while the charm quark annihilation effects are neglected owing to the OZI rule.

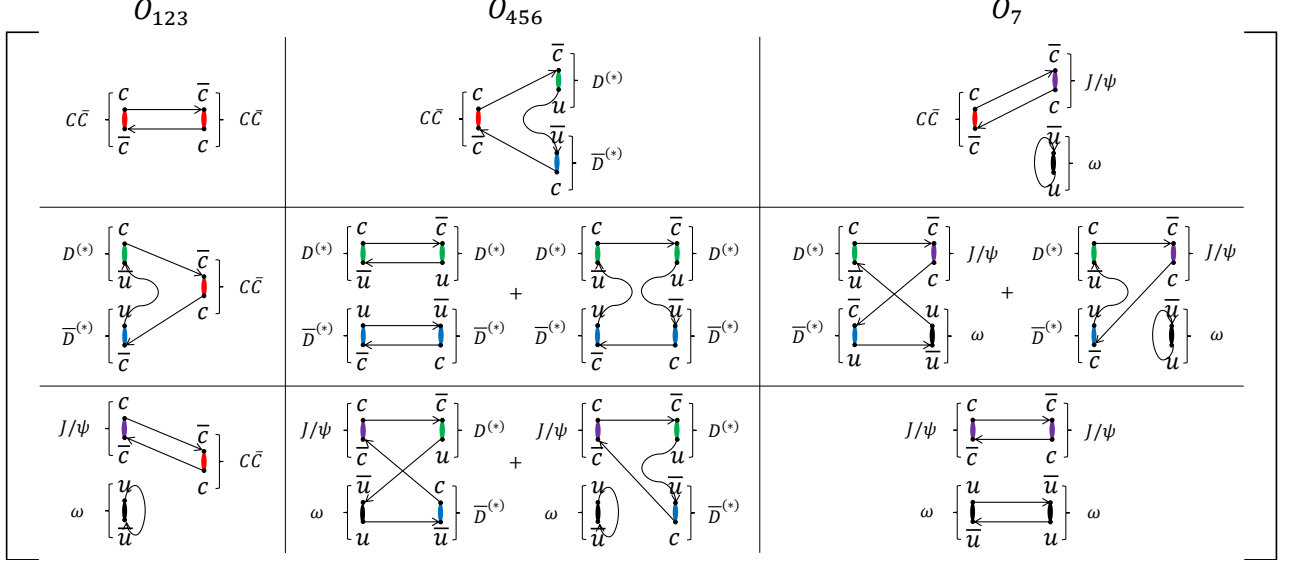


FIG. A1. Schematic quark contraction diagrams for the calculation of the correlation matrix $C_{\alpha\beta}(t)$. For convenience, the operator set is sorted as $\{\mathcal{O}_\alpha|\alpha = 1, \dots, 7\} = \{\mathcal{O}_{c\bar{c}}^{r=0}, \mathcal{O}_{c\bar{c}}^{r=1}, \mathcal{O}_{c\bar{c}}^{r=2}, \mathcal{O}_{D\bar{D}}^{q=0, \gamma 5}, \mathcal{O}_{D\bar{D}}^{q=0, \gamma 4 \gamma 5}, \mathcal{O}_{D\bar{D}}^{q=1}, \mathcal{O}_{J/\psi\omega}^{q=0}\}$. All the contributions are considered except for charm quark annihilation diagrams which are expected to be suppressed by the OZI rule.

TABLE A1. Energy levels E_n from different subsets of operators for lattice ensemble $m_\pi = 250$ MeV. In each row of E_n , the energy values (converted to the physical unit GeV through the fixed a_t^{-1} in Table C1) are obtained from the operators in the non-empty columns. Therefore, the first four rows of E_n show the unmixed energies. The mixing effects are very weak and can almost be neglected for $DD^*(q=0) - DD^*(q=1)$ (row no.5), $J/\psi\omega - DD^*$ (row no.6) and $J/\psi\omega - c\bar{c}$ (row no.7) mixings. The strong mixing takes place between $c\bar{c}$ states and DD^* states, which is manifested by the substantial changes of energies E_2 and E_3 after the mixing (row no.8 and row no.9).

\mathcal{O}_α	$\mathcal{O}_{1,2,3}$			$\mathcal{O}_4(DD^*, q=0)$	$\mathcal{O}_5(DD^*, q=0)$	$\mathcal{O}_6(DD^*, q=1)$	$\mathcal{O}_7(J/\psi\omega, q=0)$
n	1	3	5	2	4	6	-
$E_n(\text{GeV})$	3.4907(20)	3.9082(47)	4.087(54)				
	3.4907(20)	3.9082(47)	4.087(54)				3.889(13)
				3.5099(65)	4.142(22)	4.215(49)	
				3.5099(65)	4.142(22)	4.215(49)	3.889(13)
	3.4896(19)	3.9282(46)	4.089(55)	3.8324(36)	4.0308(49)	4.577(14)	3.889(13)
	3.4896(19)	3.9282(46)	4.089(55)	3.8324(36)	4.0308(49)	4.577(14)	

First, we take the following procedure to check the relevance of individual operators $\mathcal{O}_\alpha \in \mathcal{S}$ to the DD^* scattering we are interested in:

- We start with the subset $\{\mathcal{O}_1, \mathcal{O}_2, \mathcal{O}_3\}$ ($c\bar{c}$ operators) of \mathcal{S} , whose correlation matrix $\{C_{ij}(t), i, j = 1, 2, 3\}$ is actually a submatrix $\{C_{ij}, i, j = 1, 2, 3\}$ of $C_{\alpha\beta}(t)$. We solve the generalized eigenvalue problem (GEVP) to the submatrices of $C_{ij}(t)$,

$$C_{ij}(t_1)v_j^{(n)}(t_1, t_0) = \lambda^{(n)}(t_1, t_0)C_{ij}(t_0)v_j^{(n)}(t_1, t_0), \quad (\text{B3})$$

for given t_1, t_0 . Thus we obtain the optimized correlation functions $C^{(n)}(t) = v_i^{(n)}(t_1, t_0)v_j^{(n)}(t_1, t_0)C_{ij}(t)$. This procedure runs over the cases at the four m_π 's. The effective

masses of $C^{(1)}(t)$ and $C^{(2)}(t)$ are illustrated in the rightmost column (column (e)) in each panel of Fig. A2. When $\mathcal{O}_7(J/\psi\omega, q=0)$ is added to the operator subset, the solution to the corresponding GEVP gives an additional energy level close to the $J/\psi\omega$ threshold, as shown in column (c) as black points in each panel of Fig. A2.

- Now we perform the GEVP analysis to the operator subset $\{\mathcal{O}_4, \mathcal{O}_5, \mathcal{O}_6, \mathcal{O}_7\}$. The effective masses of the four optimized correlation functions are plotted in column (d) of each panel of Fig. A2, where the effective mass illustrated by black points is almost the same as that in column (c). Other three effective masses have good signal-to-noise ratios but do not show plateaus even in the time range

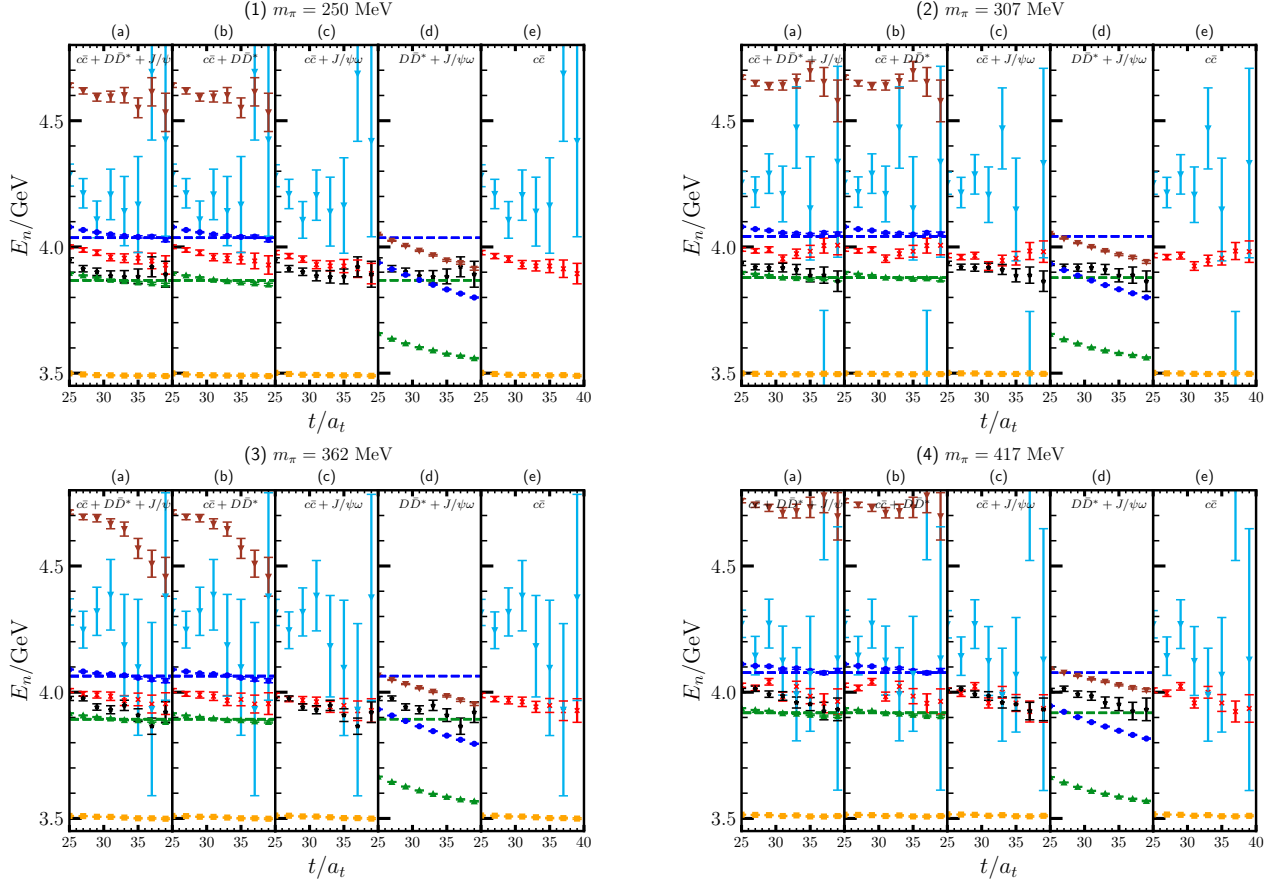


FIG. A2. Effective mass using different operators subset and solving GEVP, ranging from different m_π . In each column of the panels, the headers indicate the operators involved in GEVP. The colored lines show the effective mass behavior corresponding to their dominant operators, as indicated by the same color. Their fitting values are given in Table.[A1-A4].

TABLE A2. Similar to Tab. A1 but for $m_\pi = 307$ MeV.

\mathcal{O}_α	$\mathcal{O}(r=0, a_s, 2a_s)$			$\mathcal{O}_{D\bar{D}^*}^1(q=0)$	$\mathcal{O}_{D\bar{D}^*}^2(q=0)$	$\mathcal{O}_{D\bar{D}^*}^1(q=1)$	$J/\psi\omega$
n	1	3	5	2	4	6	-
$E_n(\text{GeV})$	3.4947(20)	3.9135(47)	4.178(45)				3.878(13)
	3.4947(20)	3.9135(47)	4.178(45)				
				3.5180(67)	4.135(24)	4.133(47)	
				3.5180(67)	4.135(24)	4.133(47)	3.878(13)
	3.4935(19)	3.9343(43)	4.182(45)	3.8461(33)	4.0411(36)	4.619(13)	3.878(13)
	3.4935(19)	3.9343(43)	4.182(45)	3.8461(33)	4.0411(36)	4.619(13)	

$t/a_t \in [25, 40]$.

- If the GEVP analysis is performed to the full operator set \mathcal{S} , we obtain seven optimized correlation functions. The effective masses of the lowest six states are plotted in column (a) of each panel of Fig. A2. One can see that the effective masses of the lowest five states tend to saturate on plateaus. Column (b) in each panel of Fig. A2 shows the effective masses when the $J/\psi\omega$ operator is excluded from the operator set. In comparison

with column (a), the state illustrated by black points disappears but other states are still there and almost do not change.

The observations above indicate that the $J/\psi\omega$ operator (\mathcal{O}_7) almost does not couple with $c\bar{c}$ and $D\bar{D}^*$ operators and are therefore nearly irrelevant to the $D\bar{D}^*$ scattering. In contrast, $c\bar{c}$ and $D\bar{D}^*$ operators strongly couple with each other and must be considered together. These observations are in agreement with the previous work Ref. [28].

TABLE A3. Similar to Tab. A1 but for $m_\pi = 362$ MeV.

\mathcal{O}_α	$\mathcal{O}(r=0, a_s, 2a_s)$			$\mathcal{O}_{D\bar{D}^*}^1(q=0)$	$\mathcal{O}_{D\bar{D}^*}^2(q=0)$	$\mathcal{O}_{D\bar{D}^*}^1(q=1)$	$J/\psi\omega$
n	1	3	5	2	4	6	-
$E_n(\text{GeV})$	3.5021(23)	3.9528(44)	4.242(41)				3.923(10)
	3.5021(23)	3.9528(44)	4.242(41)				
				3.5208(61)	4.131(21)	4.187(37)	
				3.5208(61)	4.131(21)	4.187(37)	3.923(10)
	3.5018(21)	3.9680(40)	4.245(41)	3.8687(26)	4.0589(36)	4.688(11)	3.923(10)
	3.5018(21)	3.9680(40)	4.245(41)	3.8687(26)	4.0589(36)	4.688(11)	

TABLE A4. Similar to Tab. A1 but for $m_\pi = 417$ MeV.

\mathcal{O}_α	$\mathcal{O}(r=0, a_s, 2a_s)$			$\mathcal{O}_{D\bar{D}^*}^1(q=0)$	$\mathcal{O}_{D\bar{D}^*}^2(q=0)$	$\mathcal{O}_{D\bar{D}^*}^1(q=1)$	$J/\psi\omega$
n	1	3	5	2	4	6	-
$E_n(\text{GeV})$	3.5089(21)	3.9778(43)	4.121(73)				3.9688(77)
	3.5089(21)	3.9778(43)	4.121(73)				
				3.5320(55)	4.179(24)	4.348(70)	
				3.5320(55)	4.179(24)	4.348(70)	3.9688(77)
	3.5083(20)	3.9934(41)	4.123(74)	3.8949(24)	4.0850(27)	4.720(11)	3.9688(77)
	3.5083(20)	3.9934(41)	4.123(74)	3.8949(24)	4.0850(27)	4.720(11)	

As for the energy levels E_n to be determined, we take the convention that the energy levels reflected by the effective masses in column (b) of Fig. A2 are ordered as E_1, E_2, \dots, E_6 from bottom to top. For a specific subset of the full operator set \mathcal{S} , the energy level that is adjacent to E_n has the same index n . We do not include the energy level (indicated by black points) corresponding to the $J/\psi\omega$ to the level order.

For each specific operator subset, we first perform two-exponential fits to the optimized correlation functions $C^{(n)}(t)$ introduced above and take the lowest energy to be an estimate of E_n , which are listed in Tables A1-A4 for all the four m_π 's. In the data blocks in each table, the first two rows of the leftmost block are almost the same and are the energy levels E_n from $c\bar{c}$ operators with and without the $J/\psi\omega$ operator. The energies E_n in the first two rows of the middle block are from $D\bar{D}^*$ operators with and without the $J/\psi\omega$ operator. The energies E_n in the last two rows are from both $c\bar{c}$ and $D\bar{D}^*$ operators (with and without the $J/\psi\omega$ operator). The energy values in bold are determined from the ratio method (see below). It is seen that the inclusion or exclusion of the $J/\psi\omega$ operator almost does not affect other energy values. So we exclude the $J/\psi\omega$ operator in the following discussions.

Comparing the energy levels from only $c\bar{c}$ operators, those from only $D\bar{D}^*$ operators, and those from both $c\bar{c}$ and $D\bar{D}^*$ operators, the strong correlation between $c\bar{c}$ and $D\bar{D}^*$ operators is obviously manifested. Especially, the three energy levels from only $D\bar{D}^*$ operators are far from non-interacting $D\bar{D}^*$ energies. This is attributed to

the light quark annihilation effects illustrated in Fig. A1. Therefore, it is necessary to include $c\bar{c}$ operators when the $I = 0$ $D\bar{D}^*$ scattering is considered. In this sense, the energies E_n (the bottom row in Tables A1-A4) from both $c\bar{c}$ and $D\bar{D}^*$ operators are taken as good estimates of the eigenvalues of the lattice Hamiltonian relevant to the $I^G J^{PC} = 0^+ 1^{++}$ charmonium-like system.

To be specific, we determine the finite volume energies based on the correlation matrix of $c\bar{c}$ and $D\bar{D}^*$ operators, which compose an operator set $\tilde{\mathcal{S}} = \{\mathcal{O}_\alpha | \alpha = 1, \dots, 6\} = \{\mathcal{O}_{c\bar{c}}^{r=0}, \mathcal{O}_{c\bar{c}}^{r=1}, \mathcal{O}_{c\bar{c}}^{r=2}, \mathcal{O}_{D\bar{D}^*}^{q=0, \gamma_5}, \mathcal{O}_{D\bar{D}^*}^{q=0, \gamma_4 \gamma_5}, \mathcal{O}_{D\bar{D}^*}^{q=1}\}$. By solving the GEVP to the corresponding correlation matrix $C_{\alpha\beta}(t)$ similarly to Eq. (B3), we obtain six eigenvectors $\{v_\alpha^{(n)}, n = 1, 2, \dots, 6\}$ and six optimized correlation functions $\{C^{(n)}(t) = v_\alpha^{(n)} v_\beta^{(n)} C_{\alpha\beta}(t), n = 1, 2, \dots, 6\}$. It is expected that $C^{(n)}(t)$ is contributed most from the n -th eigenstate with the eigen-energy E_n of the lattice Hamiltonian. The physical status of these states can be explored qualitatively by the coupling factor $Z_\alpha^{(n)}$ of \mathcal{O}_α to the n -th state, which is extracted through the expression

$$Z_\alpha^{(n)} \equiv |\langle 0 | \mathcal{O}_\alpha | n \rangle| \approx \frac{\sqrt{2E_n} C_{\alpha\beta}(t^*) v_\beta^{(n)}}{\sqrt{v_\beta^{(n)} v_\gamma^{(n)} C_{\beta\gamma}(t^*) e^{-E_n t^*}}} \quad (\text{B4})$$

at t^* where the effective mass plateaus are almost reached. The relative coupling factors $Z_\alpha^{(n)}$ (normalized by the maximal value of $Z_\alpha^{(n)}$ for each operator \mathcal{O}_α) are shown in Fig. B1. Obviously, the $c\bar{c}$ operators $\mathcal{O}_{1,2,3}$ couple most to the E_1 state and also have substantial

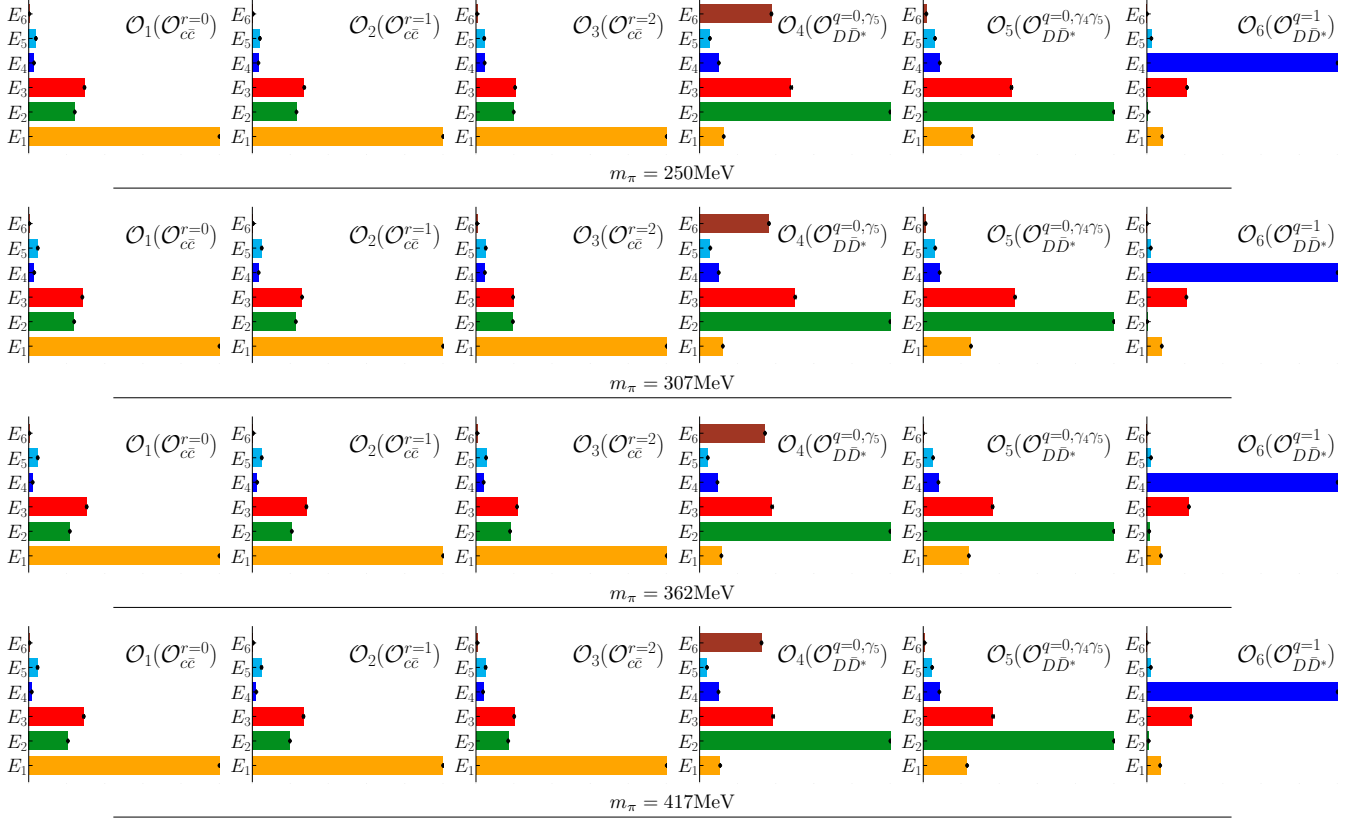


FIG. B1. Relative couplings $Z_\alpha^{(n)} = \langle 0 | \mathcal{O}_\alpha | n \rangle$ at various m_π . For each operator \mathcal{O}_α , $Z_\alpha^{(n)}$ is normalized by the largest value in $\{Z_\alpha^{(n)}, n = 1, 2, \dots, 6\}$. For each state $|n\rangle$, $\{Z_\alpha^{(n)}, \alpha = 1, 2, \dots, 6\}$ (in the same color) signal the relative importance of $c\bar{c}$ and $D\bar{D}^*$ components.

overlaps to the E_2 and E_3 states. In contrast, $\mathcal{O}_{4,5}$ ($D\bar{D}^*$ operators with $q = 0$) couple mainly to E_2 , and also overlap substantially to E_1 and E_3 states. \mathcal{O}_4 also has a large overlap to E_6 . \mathcal{O}_6 ($\mathcal{O}_{D\bar{D}^*}(q = 1)$ operator) couples predominantly to E_4 and has a sizable coupling to the E_3 state. Based on these information, we make the following raw identification:

- The E_1 state of an energy around 3.5 GeV is unambiguously assigned to be the conventional $\chi_{c1}(1P)$ state.
- The E_6 state is coupled mainly by the $D\bar{D}^*(q = 0)$ operator, but has very high energy around 4.6-4.7 GeV (see the bottom rows of Tables A1-A4). According to the experimental evidence the mass splitting of $1S - 2S$ mesons are usually around 600 MeV, the E_6 state is very likely composed of a ground $D^{(*)}$ state and an excited $\bar{D}^{(*)}$ state with relative zero momentum.
- The values of E_5 have fairly large errors and are insensitive to the inclusion or exclusion of $D\bar{D}^*$ operator. On the other hand, E_5 is relatively far from the energy region relevant to $X(3872)$, so we do not pay much attention to it.

- The E_2, E_3, E_4 states are very relevant to $D\bar{D}^*$ scattering and $X(3872)$, therefore it is very crucial for them to be determined as precisely as possible.

Appendix C: Systematic uncertainties from anisotropic lattice

To facilitate a clearer comprehension of physical values in this study, the fixed a_t^{-1} mean values are adopted to present the finite volume energies, notwithstanding the uncertainties associated with the lattice space a_s and the anisotropy parameter $\xi \equiv a_s/a_t$. Besides, a systematic uncertainty on anisotropic parameter ξ should be taken into account in finite volume scattering analysis. Generally, the finite volume scattering momenta are determined by solving the dispersion relation from prescribed energy levels,

$$E_n = \sqrt{m_D^2 + \vec{p}_n^2} + \sqrt{m_{D^*}^2 + \vec{p}_n^2},$$

$$\vec{p}_n^2 = \frac{1}{4}E_n^2 - \frac{1}{2}(m_D^2 + m_{D^*}^2) + \frac{(m_D^2 - m_{D^*}^2)^2}{4E_n^2}, \quad (\text{C1})$$

So we use several fitting methods to extract the values of $E_{2,3,4}$ and compare the results to check the self-

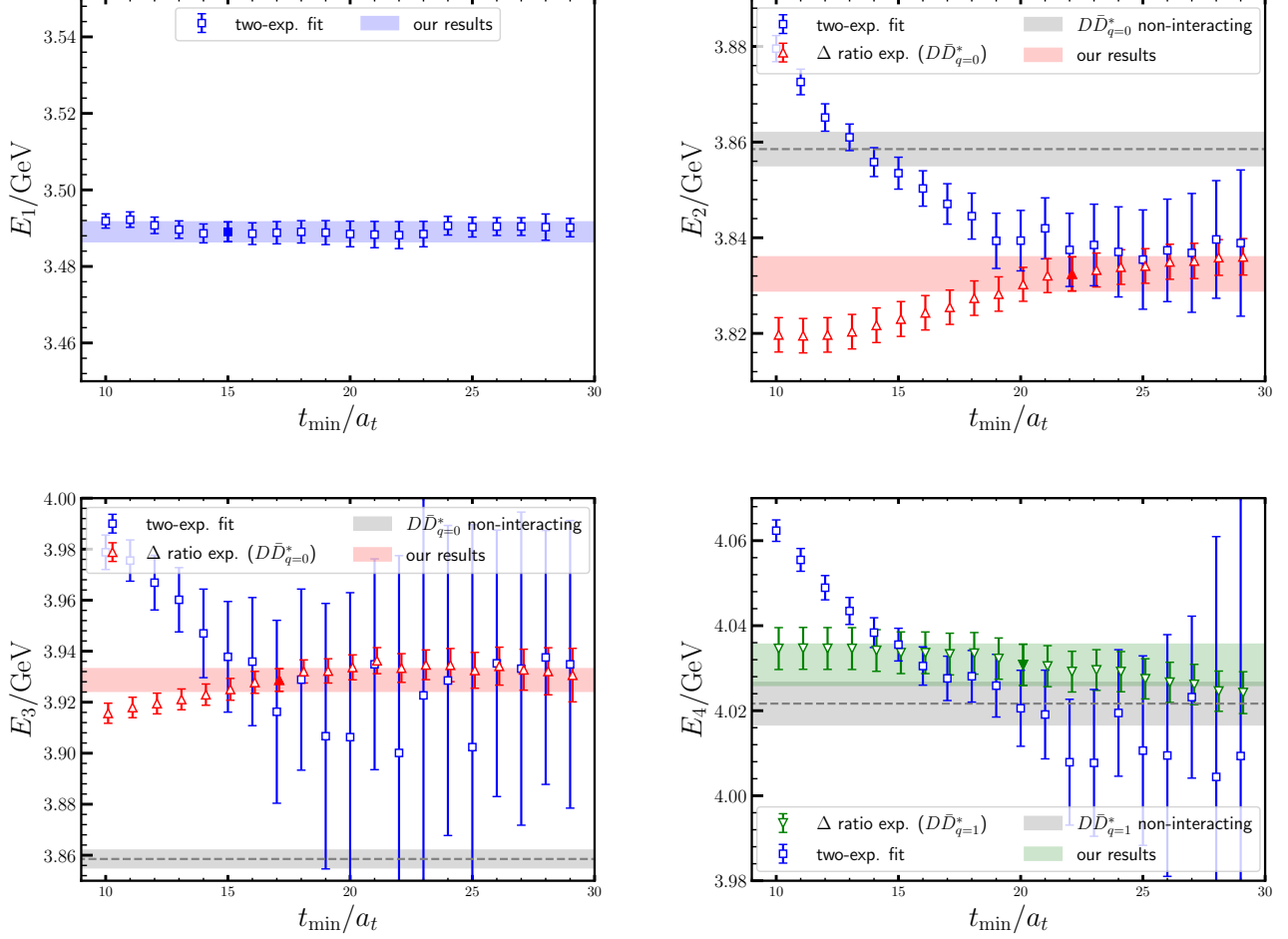


FIG. B2. The self-consistency check of the fitted $E_{1,2,3,4}$ through different methods (Fit A, Fit B or Fit C in Eq. C2) at $m_\pi = 250$ MeV. The x -axis t_{\min} denotes the different lower bounds of the fit window $[t_{\min}, t_{\max}]$ (the upper bound is fixed to be $t_{\max} = 35$). **Top left:** the fitting results of E_1 at different t_{\min} . The filled point indicates our final result. **Top right:** E_2 results. The grey band illustrates the non-interacting $D\bar{D}^*$ energy $E_{D\bar{D}^*}^{q=0}$ (the $D\bar{D}^*$ threshold). The blue points show the two-exponential fit (Fit A) results of E_2 , while the red points are the results $E_2 = E_{D\bar{D}^*}^{q=0} + \Delta_2(0)$ from the ratio method (Fit B). The results of fit A and Fit B are consistent with each other for $t_{\min}/a_t \in [15, 28]$ but the latter have quite small statistical errors. So we take Fit B result at $t_{\min}/a_t = 22$ (indicated by the filled point) as our final result for E_2 (the red band). **Bottom left:** E_3 results. The figure legends are similar to the case of E_2 . Although the consistency of the results of Fit A and Fit B, it is seen that the Fit B results have much smaller statistical errors and show little dependence on t_{\min} . So again we take Fit B result at $t_{\min}/a_t = 17$ as our final result for E_2 (the red band). **Bottom right:** E_4 results: The grey band illustrates the non-interacting $D\bar{D}^*$ energy $E_{D\bar{D}^*}^{q=0}$. The blue points illustrate the Fit A result, while the green points are the results from Fit C (the ratio method) with $E_4 = E_{D\bar{D}^*}^{q=0} + \Delta_4(1)$. The results of Fit C are consistent with the two-exponential fit (Fit A) results but have much smaller statistical errors. So we take the Fit C results at $t_{\min}/a_t = 20$ as our final results (the green band).

consistency:

$$\begin{aligned}
 \text{Fit A: } C^{(n)}(t) &= (A_1 e^{-E_n t} + A_2 e^{-E' t}) \\
 &\quad + (t \rightarrow (T - t)), \\
 \text{Fit B: } R^{(n)}(t, q=0) &= \frac{C^{(n)}(t)}{C_D(t, q=0)C_{D^*}(t, q=0)} \\
 &\approx A e^{-\Delta_n(0)t}, \\
 \text{Fit C: } R^{(n)}(t, q=1) &= \frac{C^{(n)}(t)}{C_D(t, q=1)C_{D^*}(t, q=1)} \\
 &\approx A e^{-\Delta_n(1)t}. \tag{C2}
 \end{aligned}$$

Fit A is a two-state fitting. Fit B involves fitting the two-point corrector ratio $R(t)$ that $C(t)$ over the non-interacting $C_D(t, q=0)$ and $C_{D^*}(t, q=0)$ using a single exponential function and then adding its non-interacting energy levels $E_n = E_{D\bar{D}^*}^q + \Delta_n(q)$ through the jackknife analysis. Fit C is similar to Fit B but accounts for the non-interacting $C_D(t, q=1)$ and $C_{D^*}(t, q=1)$. The comparisons are illustrated in Figs. B2-B5 for the four m_π 's. In each figure, the top-left panel shows the fitted results of E_1 at different t_{\min} of the fit window

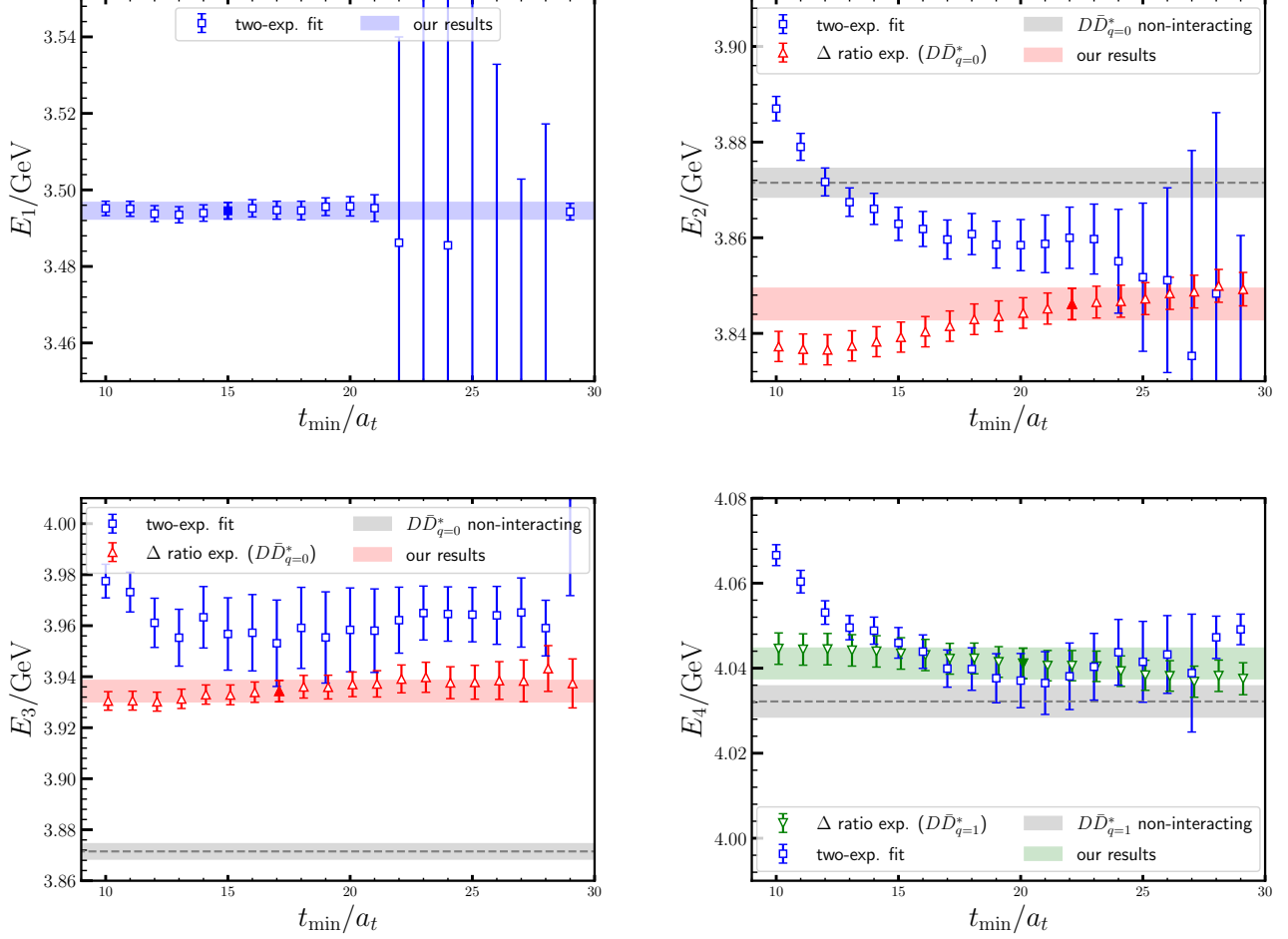


FIG. B3. The self-consistency check of the fitted $E_{1,2,3,4}$ through different methods at $m_\pi = 307$ MeV. The layout is similar to Fig. B2. The filled point in each panel indicates the t_{\min}/a_t where our final result is taken.

$[t_{\min}, t_{\max}]$. The maximum timeslice range t_{\max} is set to 40 across all fits, as this is in the saturation range of these observed energy levels.

- In the case of energy level E_1 , it is far below the $D\bar{D}^*$ threshold, and the simple two-states fitting performs well enough, while the ratio-exponential fits are unflavored due to the substantial effects of excited states artifacts.
- The energy level E_2 is slightly below $D\bar{D}^*$ threshold about 20 MeV. The results from Fit A and Fit B reach commendable consistency.
- For energy level E_3 , the results from Fit B show greater precision compared to Fit A (two-state fit). Consequently, the results from Fit B are adopted in our determination.
- In the case of energy level E_4 , Fit B (at relative momentum $q = 0$) gives unstable results, as observed the energy level plateau exhibits a gradual

slope, which suggests the potential contamination of excited states. Conversely, Fit C is observed to give a more robust and dependable result for the energy plateau.

Practically, the dimensionless scattering momenta are derived from the relation $q^2 = (\frac{2\pi}{L\xi})^2 (a_t \vec{p})^2$, where $(a_t \vec{p})^2$ expressed in lattice unit. In such a relation, it is necessary to take into account the uncertainty of the anisotropy parameter caused by solving the dimensionless scattering momenta. Since this study focuses on the $D\bar{D}^*$ channel, We choose to employ the anisotropy parameter measured from D and D^* meson. Given the slight deviation observed in the dispersion relations of the D and D^* mesons, as documented in Table C1, we incorporate this discrepancy as a source of systematic uncertainty. The determined values ξ_{sys} . ensure that the one-sigma uncertainty range encompasses these systematic variations.

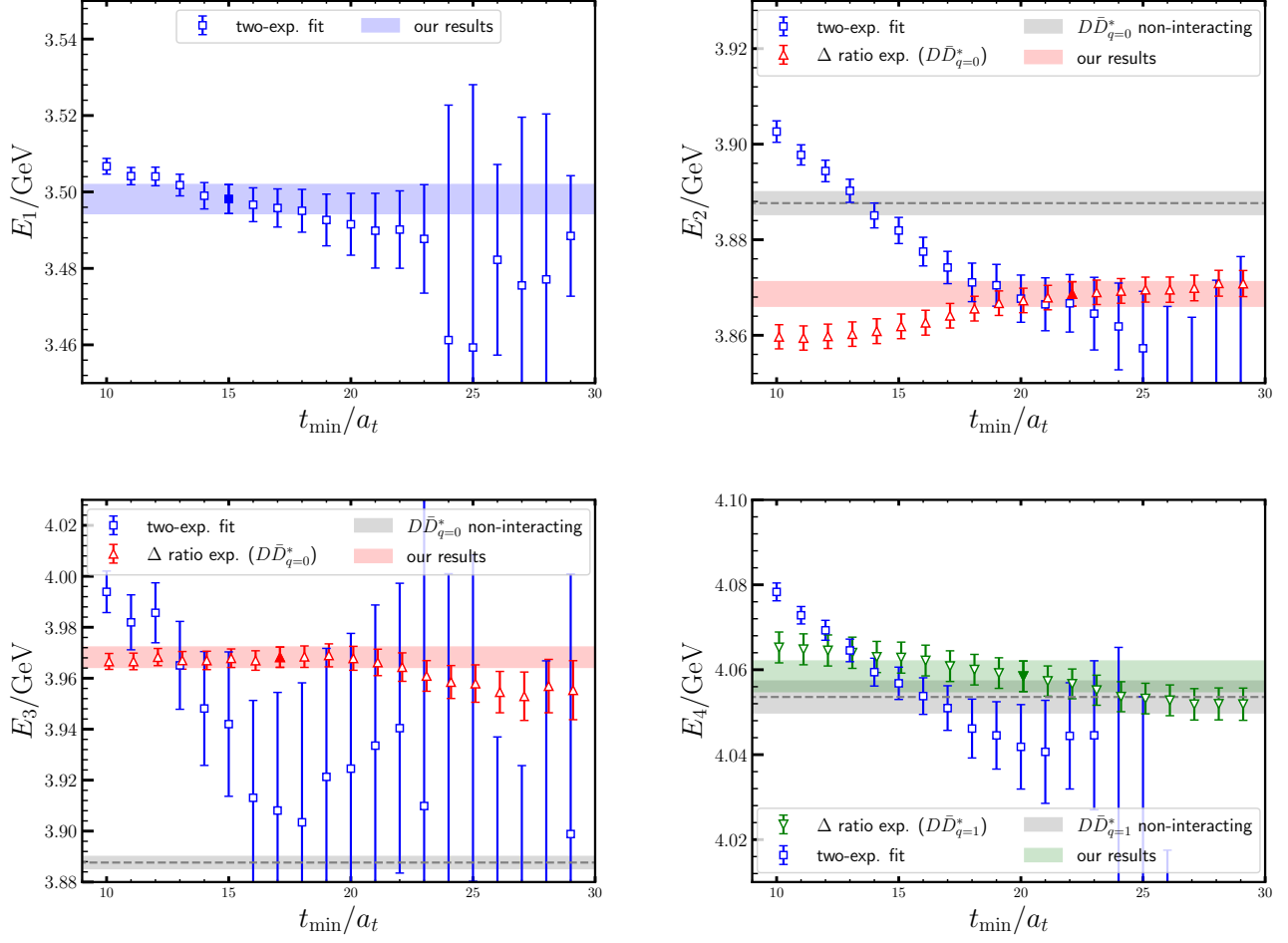


FIG. B4. The self-consistency check of the fitted $E_{1,2,3,4}$ through different methods at $m_\pi = 362$ MeV. The layout is similar to Fig. B2. The filled point in each panel indicates the t_{\min}/a_t where our final result is taken.

TABLE C1. Anisotropy parameter ξ and dispersion relation of various ensembles. The derivation of ξ_D and ξ_{D^*} is considered to be a systematic uncertainty in Eq. (C1), noted as $\xi_{\text{sys.}}$.

ens.	m_π/MeV	a_t^{-1}/GeV	$\xi_{J/\psi}$	ξ_D	ξ_{D^*}	$\xi_{\text{sys.}}$
M245	250(3)	7.276	5.061 (10)	5.070 (22)	5.126 (54)	5.11(7)
M305	307(2)	7.187	5.083 (10)	5.025 (16)	5.068 (30)	5.05(5)
M360	362(1)	7.187	4.989 (10)	4.974 (14)	4.990 (31)	4.99(3)
M415	417(1)	7.219	5.021 (11)	5.031 (16)	5.091 (39)	5.07(6)

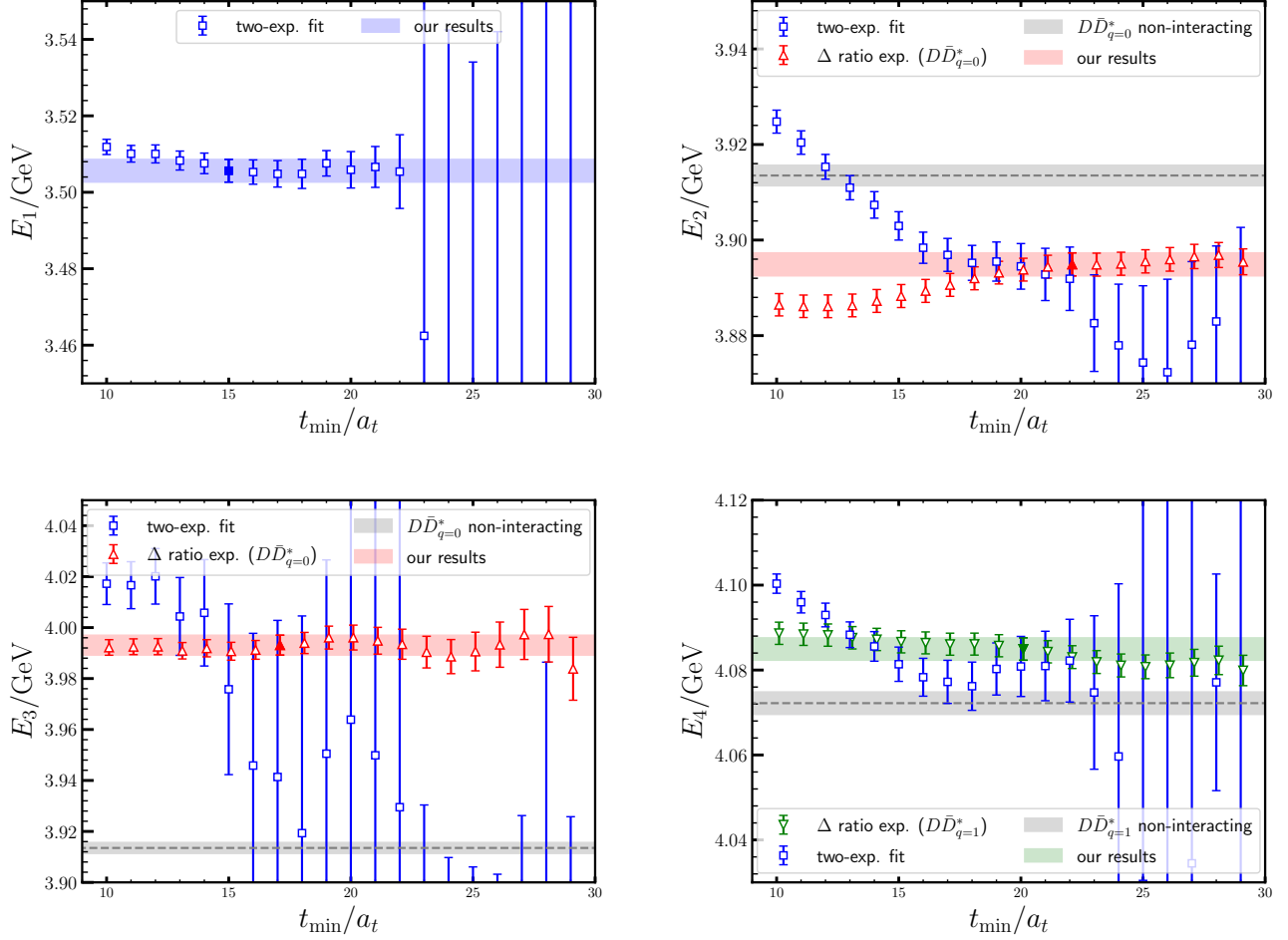


FIG. B5. The self-consistency check of the fitted $E_{1,2,3,4}$ through different methods at $m_\pi = 417$ MeV. The layout is similar to Fig. B2. The filled point in each panel indicates the t_{\min}/a_t where our final result is taken.

- [1] S. K. Choi *et al.* (Belle), “Observation of a Narrow Charmonium-like state in Exclusive $B^\pm \rightarrow K^\pm \pi^+ \pi^- J/\psi$ Decays,” *Phys. Rev. Lett.* **91**, 262001 (2003), arXiv:hep-ex/0309032.
- [2] R. L. Workman *et al.* (Particle Data Group), “Review of Particle Physics,” *PTEP* **2022**, 083C01 (2022).
- [3] R. Aaij *et al.* (LHCb), “Determination of the $X(3872)$ Meson Quantum Numbers,” *Phys. Rev. Lett.* **110**, 222001 (2013), arXiv:1302.6269 [hep-ex].
- [4] S. Godfrey and Nathan Isgur, “Mesons in a relativized quark model with chromodynamics,” *Phys. Rev. D* **32**, 189–231 (1985).
- [5] T. Barnes, S. Godfrey, and E. S. Swanson, “Higher charmonia,” *Phys. Rev. D* **72**, 054026 (2005), arXiv:hep-ph/0505002.
- [6] Nils A. Tornqvist, “Isospin breaking of the narrow charmonium state of Belle at 3872 MeV as a deuson,” *Phys. Lett. B* **590**, 209–215 (2004), arXiv:hep-ph/0402237.
- [7] Yan-Rui Liu, Xiang Liu, Wei-Zhen Deng, and Shi-Lin Zhu, “Is $X(3872)$ really a molecular state?” *Eur. Phys. J. C* **56**, 63–73 (2008), arXiv:0801.3540 [hep-ph].
- [8] Xiang Liu, Zhi-Gang Luo, Yan-Rui Liu, and Shi-Lin Zhu, “ $X(3872)$ and other possible heavy molecular states,” *Eur. Phys. J. C* **61**, 411–428 (2009), arXiv:0808.0073 [hep-ph].
- [9] Ning Li and Shi-Lin Zhu, “Isospin breaking, coupled-channel effects and $X(3872)$,” *Phys. Rev. D* **86**, 074022 (2012), arXiv:1207.3954 [hep-ph].
- [10] Lin Qiu, Chang Gong, and Qiang Zhao, “Coupled-channel description of charmed heavy hadronic molecules within the meson-exchange model and its implication,” *Phys. Rev. D* **109**, 076016 (2024), arXiv:2311.10067 [hep-ph].
- [11] Xiang-Kun Dong, Feng-Kun Guo, and Bing-Song Zou, “A survey of heavy-antiheavy hadronic molecules,” *Progr. Phys.* **41**, 65–93 (2021), arXiv:2101.01021 [hep-ph].
- [12] Eric Braaten and Masaoki Kusunoki, “Low-energy universality and the new charmonium resonance at 3870 MeV,” *Phys. Rev. D* **69**, 074005 (2004), arXiv:hep-ph/0311147.
- [13] Yu. S. Kalashnikova, “Coupled-channel model for charmonium levels and an option for $X(3872)$,” *Phys. Rev. D* **72**, 034010 (2005), arXiv:hep-ph/0506270.
- [14] T. Barnes and E. S. Swanson, “Hadron loops: General theorems and application to charmonium,” *Phys. Rev. C* **77**, 055206 (2008), arXiv:0711.2080 [hep-ph].
- [15] P. G. Ortega, J. Segovia, D. R. Entem, and F. Fernandez, “Coupled channel approach to the structure of the $X(3872)$,” *Phys. Rev. D* **81**, 054023 (2010), arXiv:0907.3997 [hep-ph].
- [16] Bai-Qing Li, Ce Meng, and Kuang-Ta Chao, “Coupled-channel and screening effects in charmonium spectrum,” *Phys. Rev. D* **80**, 014012 (2009), arXiv:0904.4068 [hep-ph].
- [17] V. Baru, C. Hanhart, Yu. S. Kalashnikova, A. E. Kudryavtsev, and A. V. Nefediev, “Interplay of quark and meson degrees of freedom in a near-threshold resonance,” *Eur. Phys. J. A* **44**, 93–103 (2010), arXiv:1001.0369 [hep-ph].
- [18] Yasuhiro Yamaguchi, Atsushi Hosaka, Sachiko Takeuchi, and Makoto Takizawa, “Heavy hadronic molecules with pion exchange and quark core couplings: a guide for practitioners,” *J. Phys. G* **47**, 053001 (2020), arXiv:1908.08790 [hep-ph].
- [19] L. Maiani, F. Piccinini, A. D. Polosa, and V. Riquer, “Diquark-antidiquark states with hidden or open charm and the nature of $X(3872)$,” *Phys. Rev. D* **71**, 014028 (2005), arXiv:hep-ph/0412098.
- [20] D. Ebert, R. N. Faustov, and V. O. Galkin, “Masses of heavy tetraquarks in the relativistic quark model,” *Phys. Lett. B* **634**, 214–219 (2006), arXiv:hep-ph/0512230.
- [21] N. Brambilla *et al.*, “Heavy quarkonium: progress, puzzles, and opportunities,” *Eur. Phys. J. C* **71**, 1534 (2011), arXiv:1010.5827 [hep-ph].
- [22] Hua-Xing Chen, Wei Chen, Xiang Liu, and Shi-Lin Zhu, “The hidden-charm pentaquark and tetraquark states,” *Phys. Rept.* **639**, 1–121 (2016), arXiv:1601.02092 [hep-ph].
- [23] A. Esposito, A. Pilloni, and A. D. Polosa, “Multi-quark resonances,” *Phys. Rept.* **668**, 1–97 (2017), arXiv:1611.07920 [hep-ph].
- [24] Feng-Kun Guo, Christoph Hanhart, Ulf-G. Meißner, Qian Wang, Qiang Zhao, and Bing-Song Zou, “Hadronic molecules,” *Rev. Mod. Phys.* **90**, 015004 (2018), [Erratum: Rev.Mod.Phys. 94, 029901 (2022)], arXiv:1705.00141 [hep-ph].
- [25] Nora Brambilla, Simon Eidelman, Christoph Hanhart, Alexey Nefediev, Cheng-Ping Shen, Christopher E. Thomas, Antonio Vairo, and Chang-Zheng Yuan, “The XYZ states: Experimental and theoretical status and perspectives,” *Phys. Rept.* **873**, 1–154 (2020), arXiv:1907.07583 [hep-ex].
- [26] Yan-Rui Liu, Hua-Xing Chen, Wei Chen, Xiang Liu, and Shi-Lin Zhu, “Pentaquark and Tetraquark states,” *Prog. Part. Nucl. Phys.* **107**, 237–320 (2019), arXiv:1903.11976 [hep-ph].
- [27] Gunnar S. Bali, Sara Collins, and Christian Ehmman, “Charmonium spectroscopy and mixing with light quark and open charm states from $n_F = 2$ lattice QCD,” *Phys. Rev. D* **84**, 094506 (2011), arXiv:1110.2381 [hep-lat].
- [28] Sasa Prelovsek and Luka Leskovec, “Evidence for $X(3872)$ from DD^* Scattering on the Lattice,” *Phys. Rev. Lett.* **111**, 192001 (2013), arXiv:1307.5172 [hep-lat].
- [29] M. Padmanath, C. B. Lang, and Sasa Prelovsek, “ $X(3872)$ and $Y(4140)$ using diquark-antidiquark operators with lattice QCD,” *Phys. Rev. D* **92**, 034501 (2015), arXiv:1503.03257 [hep-lat].
- [30] Mohammad T. AlFiky, Fabrizio Gabbiani, and Alexey A. Petrov, “ $X(3872)$: Hadronic molecules in effective field theory,” *Phys. Lett. B* **640**, 238–245 (2006), arXiv:hep-ph/0506141.
- [31] Miguel Albaladejo, Carlos Hidalgo-Duque, Juan Nieves, and Eulogio Oset, “Hidden charm molecules in finite volume,” *Phys. Rev. D* **88**, 014510 (2013), arXiv:1304.1439 [hep-lat].
- [32] V. Baru, E. Epelbaum, A. A. Filin, C. Hanhart, U. G. Meißner, and A. V. Nefediev, “Quark mass dependence of the $X(3872)$ binding energy,” *Phys. Lett. B* **726**, 537–543 (2013), arXiv:1306.4108 [hep-ph].
- [33] P. Wang and X. G. Wang, “Study on $X(3872)$ from Effective Field Theory with Pion-Exchange Interaction,”

- Phys. Rev. Lett. **111**, 042002 (2013), arXiv:1304.0846 [hep-ph].
- [34] M. Lüscher, “Volume dependence of the energy spectrum in massive quantum field theories. II. Scattering states,” *Commun. Math. Phys.* **105**, 153–188 (1986).
- [35] M. Lüscher, “Two-particle states on a torus and their relation to the scattering matrix,” *Nucl. Phys. B* **354**, 531–578 (1991).
- [36] M. Lüscher, “Signatures of unstable particles in finite volume,” *Nucl. Phys. B* **364**, 237–251 (1991).
- [37] Michael Peardon, John Bulava, Justin Foley, Colin Morningstar, Jozef Dudek, Robert G. Edwards, Balint Joo, Huey-Wen Lin, David G. Richards, and Keisuke Jimmy Juge (Hadron Spectrum), “Novel quark-field creation operator construction for hadronic physics in lattice QCD,” *Phys. Rev. D* **80**, 054506 (2009), arXiv:0905.2160 [hep-lat].
- [38] Colin J. Morningstar and Mike J. Peardon, “Efficient glueball simulations on anisotropic lattices,” *Phys. Rev. D* **56**, 4043–4061 (1997), arXiv:hep-lat/9704011.
- [39] Y. Chen *et al.*, “Glueball spectrum and matrix elements on anisotropic lattices,” *Phys. Rev. D* **73**, 014516 (2006), arXiv:hep-lat/0510074.
- [40] Jun-hua Zhang and Chuan Liu, “Tuning the tadpole improved clover Wilson action on coarse anisotropic lattices,” *Mod. Phys. Lett. A* **16**, 1841–1847 (2001), arXiv:hep-lat/0107005.
- [41] Shi-quan Su, Liu-ming Liu, Xin Li, and Chuan Liu, “A Numerical study of improved quark actions on anisotropic lattices,” *Int. J. Mod. Phys. A* **21**, 1015–1032 (2006), arXiv:hep-lat/0412034.
- [42] Guo-Zhan Meng *et al.* (CLQCD), “Low-energy $D^{*+}\bar{D}_1^0$ scattering and the resonancelike structure $Z^+(4430)$,” *Phys. Rev. D* **80**, 034503 (2009), arXiv:0905.0752 [hep-lat].
- [43] Martin Lüscher, “Properties and uses of the Wilson flow in lattice QCD,” *JHEP* **08**, 071 (2010), [Erratum: *JHEP* **03**, 092 (2014)], arXiv:1006.4518 [hep-lat].
- [44] Szabolcs Borsányi, Stephan Dürr, Zoltán Fodor, Christian Kurth, Laurent Lellouch, Thomas Lippert, and Craig McNeile (BMW), “High-precision scale setting in lattice QCD,” *JHEP* **09**, 010 (2012), arXiv:1203.4469 [hep-lat].
- [45] S. Aoki *et al.* (CP-PACS), “Lattice QCD calculation of the ρ meson decay width,” *Phys. Rev. D* **76**, 094506 (2007), arXiv:0708.3705 [hep-lat].
- [46] John Bulava *et al.* (Baryon Scattering (BaSc)), “Lattice QCD study of $\pi\Sigma - \bar{K}N$ scattering and the $\Lambda(1405)$ resonance,” *Phys. Rev. D* **109**, 014511 (2024), arXiv:2307.13471 [hep-lat].
- [47] John Bulava *et al.* (Baryon Scattering (BaSc)), “Two-Pole Nature of the $\Lambda(1405)$ Resonance from Lattice QCD,” *Phys. Rev. Lett.* **132**, 051901 (2024), arXiv:2307.10413 [hep-lat].
- [48] M. Padmanath and S. Prelovsek, “Signature of a Doubly Charm Tetraquark Pole in DD^* Scattering on the Lattice,” *Phys. Rev. Lett.* **129**, 032002 (2022), arXiv:2202.10110 [hep-lat].
- [49] D. Ebert, R. N. Faustov, and V. O. Galkin, “Properties of heavy quarkonia and B_c mesons in the relativistic quark model,” *Phys. Rev. D* **67**, 014027 (2003), arXiv:hep-ph/0210381.
- [50] Bai-Qing Li and Kuang-Ta Chao, “Higher charmonia and X, Y, Z states with screened potential,” *Phys. Rev. D* **79**, 094004 (2009), arXiv:0903.5506 [hep-ph].
- [51] Wei-Jun Deng, Hui Liu, Long-Cheng Gui, and Xian-Hui Zhong, “Charmonium spectrum and their electromagnetic transitions with higher multipole contributions,” *Phys. Rev. D* **95**, 034026 (2017), arXiv:1608.00287 [hep-ph].
- [52] Jun-Zhang Wang, Dian-Yong Chen, Xiang Liu, and Takayuki Matsuki, “Constructing J/ψ family with updated data of charmoniumlike Y states,” *Phys. Rev. D* **99**, 114003 (2019), arXiv:1903.07115 [hep-ph].
- [53] Siyang Chen, Chunjiang Shi, Ying Chen, Ming Gong, Zhaofeng Liu, Wei Sun, and Renqiang Zhang, “ $T_{cc}^+(3875)$ relevant DD^* scattering from $N_f = 2$ lattice QCD,” *Phys. Lett. B* **833**, 137391 (2022), arXiv:2206.06185 [hep-lat].
- [54] Meng-Lin Du, Arseniy Filin, Vadim Baru, Xiang-Kun Dong, Evgeny Epelbaum, Feng-Kun Guo, Christoph Hanhart, Alexey Nefediev, Juan Nieves, and Qian Wang, “Role of Left-Hand Cut Contributions on Pole Extractions from Lattice Data: Case Study for $T_{cc}(3875)^+$,” *Phys. Rev. Lett.* **131**, 131903 (2023), arXiv:2303.09441 [hep-ph].
- [55] Lu Meng, Vadim Baru, Evgeny Epelbaum, Arseniy A. Filin, and Ashot M. Gasparyan, “Solving the left-hand cut problem in lattice QCD: $T_{cc}(3875)^+$ from finite volume energy levels,” *Phys. Rev. D* **109**, L071506 (2024), arXiv:2312.01930 [hep-lat].
- [56] André Baião Raposo and Maxwell T. Hansen, “Finite-volume scattering on the left-hand cut,” *JHEP* **08**, 075 (2024), arXiv:2311.18793 [hep-lat].
- [57] Daniel Mohler, C. B. Lang, Luka Leskovec, Sasa Prelovsek, and R. M. Woloshyn, “ $D_{s0}^*(2317)$ Meson and D -Meson-Kaon Scattering from Lattice QCD,” *Phys. Rev. Lett.* **111**, 222001 (2013), arXiv:1308.3175 [hep-lat].
- [58] Yan Li, Feng-Kun Guo, Jin-Yi Pang, and Jia-Jun Wu, “Generalization of Weinberg’s compositeness relations,” *Phys. Rev. D* **105**, L071502 (2022), arXiv:2110.02766 [hep-ph].
- [59] F. Vidal and J. LeTourneux, “Multichannel scattering with nonlocal and confining potentials. 1: General theory,” *Phys. Rev. C* **45**, 418–429 (1992).
- [60] Yan Li and Jia-Jun Wu, “Inverse scattering problem with a bare state,” *Phys. Rev. D* **105**, 116024 (2022), arXiv:2204.05510 [hep-ph].
- [61] E. Cincioglu, J. Nieves, A. Ozpineci, and A. U. Yilmazer, “Quarkonium Contribution to Meson Molecules,” *Eur. Phys. J. C* **76**, 576 (2016), arXiv:1606.03239 [hep-ph].
- [62] Francesco Giacosa, Milena Piotrowska, and Susana Coito, “ $X(3872)$ as virtual companion pole of the charm–anticharm state $\chi_{c1}(2P)$,” *Int. J. Mod. Phys. A* **34**, 1950173 (2019), arXiv:1903.06926 [hep-ph].
- [63] Qian Deng, Ru-Hui Ni, Qi Li, and Xian-Hui Zhong, “Charmonia in an unquenched quark model,” (2023), arXiv:2312.10296 [hep-ph].
- [64] Guang-Juan Wang, Zhi Yang, Jia-Jun Wu, Makoto Oka, and Shi-Lin Zhu, “New insight into the exotic states strongly coupled with the DD^* from the T_{cc}^+ ,” (2023), arXiv:2306.12406 [hep-ph].
- [65] Jun-Zhang Wang, Zi-Yang Lin, Yan-Ke Chen, Lu Meng, and Shi-Lin Zhu, “Probing the pole origin of $X(3872)$ with the coupled-channel dynamics,” (2024), arXiv:2404.16575 [hep-ph].
- [66] Kazuo Abe *et al.* (Belle), “Observation of a Charmonium-like State Produced in Association with a J/ψ in e^+e^-

- annihilation at $\sqrt{s} \approx 10.6$ GeV,” *Phys. Rev. Lett.* **98**, 082001 (2007), [arXiv:hep-ex/0507019](#).
- [67] P. Pakhlov *et al.* (Belle), “Production of New Charmoniumlike States in $e^+e^- \rightarrow J/\psi D^{(*)} \bar{D}^{(*)}$ at $\sqrt{s} \approx 10.6$ GeV,” *Phys. Rev. Lett.* **100**, 202001 (2008), [arXiv:0708.3812 \[hep-ex\]](#).
- [68] Feng-Kun Guo, Christoph Hanhart, Ulf-G. Meißner, Qian Wang, and Qiang Zhao, “Production of the $X(3872)$ in charmonia radiative decays,” *Phys. Lett. B* **725**, 127–133 (2013), [arXiv:1306.3096 \[hep-ph\]](#).
- [69] Takumi Iritani, Sinya Aoki, Takumi Doi, Testuo Hatsuda, Yoichi Ikeda, Takashi Inoue, Noriyoshi Ishii, Hidekatsu Nemura, and Kenji Sasaki, “Are two nucleons bound in lattice QCD for heavy quark masses? Consistency check with Lüscher’s finite volume formula,” *Phys. Rev. D* **96**, 034521 (2017), [arXiv:1703.07210 \[hep-lat\]](#).
- [70] L. Castillejo, R. H. Dalitz, and F. J. Dyson, “Low’s scattering equation for the charged and neutral scalar theories,” *Phys. Rev.* **101**, 453–458 (1956).
- [71] Geoffrey F. Chew and Steven C. Frautschi, “Potential Scattering as Opposed to Scattering Associated with Independent Particles in the S-Matrix Theory of Strong Interactions,” *Phys. Rev.* **124**, 264 (1961).
- [72] Tetsuo Hyodo, Daisuke Jido, and Atsushi Hosaka, “Origin of the resonances in the chiral unitary approach,” *Phys. Rev. C* **78**, 025203 (2008), [arXiv:0803.2550 \[nucl-th\]](#).
- [73] C. Hanhart, Yu. S. Kalashnikova, and A. V. Nefediev, “Interplay of quark and meson degrees of freedom in a near-threshold resonance: multi-channel case,” *Eur. Phys. J. A* **47**, 101–110 (2011), [arXiv:1106.1185 \[hep-ph\]](#).
- [74] Yuki Kamiya and Tetsuo Hyodo, “Generalized weak-binding relations of compositeness in effective field theory,” *PTEP* **2017**, 023D02 (2017), [arXiv:1607.01899 \[hep-ph\]](#).
- [75] Zhi-Hui Guo and J. A. Oller, “Resonance on top of thresholds: the $\Lambda_c(2595)^+$ as an extremely fine-tuned state,” *Phys. Rev. D* **93**, 054014 (2016), [arXiv:1601.00862 \[hep-ph\]](#).
- [76] Xian-Wei Kang and J. A. Oller, “Different pole structures in line shapes of the $X(3872)$,” *Eur. Phys. J. C* **77**, 399 (2017), [arXiv:1612.08420 \[hep-ph\]](#).
- [77] Roel Aaij *et al.* (LHCb), “Observation of new charmonium(-like) states in $B^+ \rightarrow D^{*\pm} D^\mp K^+$ decays,” (2024), [arXiv:2406.03156 \[hep-ex\]](#).
- [78] Sasa Prelovsek, Sara Collins, Daniel Mohler, M. Padmanath, and Stefano Piemonte, “Charmonium-like resonances with $J^{PC} = 0^{++}, 2^{++}$ in coupled $D\bar{D}, D_s\bar{D}_s$ scattering on the lattice,” *JHEP* **06**, 035 (2021), [arXiv:2011.02542 \[hep-lat\]](#).
- [79] David J. Wilson, Christopher E. Thomas, Jozef J. Dudek, and Robert G. Edwards (Hadron Spectrum), “Charmonium χ_{c0} and χ_{c2} resonances in coupled-channel scattering from lattice QCD,” *Phys. Rev. D* **109**, 114503 (2024), [arXiv:2309.14071 \[hep-lat\]](#).
- [80] David J. Wilson, Christopher E. Thomas, Jozef J. Dudek, and Robert G. Edwards (Hadron Spectrum), “Scalar and Tensor Charmonium Resonances in Coupled-Channel Scattering from Lattice QCD,” *Phys. Rev. Lett.* **132**, 241901 (2024), [arXiv:2309.14070 \[hep-lat\]](#).
- [81] Robert G. Edwards and Balint Joo (SciDAC, LHPC, UKQCD), “The Chroma software system for lattice QCD,” *Nucl. Phys. B Proc. Suppl.* **140**, 832 (2005), [arXiv:hep-lat/0409003](#).
- [82] M. A. Clark, R. Babich, K. Barros, R. C. Brower, and C. Rebbi, “Solving Lattice QCD systems of equations using mixed precision solvers on GPUs,” *Comput. Phys. Commun.* **181**, 1517–1528 (2010), [arXiv:0911.3191 \[hep-lat\]](#).
- [83] R. Babich, M. A. Clark, B. Joo, G. Shi, R. C. Brower, and S. Gottlieb, “Scaling Lattice QCD beyond 100 GPUs,” in *SC11 International Conference for High Performance Computing, Networking, Storage and Analysis* (2011) [arXiv:1109.2935 \[hep-lat\]](#).